Theory of ordering dynamics for Cu_3Au

Z.-W. Lai*
The James Franck Institute and Department of Physics, The University of Chicago, Chicago, Illinois 60637
(Received 4 December 1989)

A coarse-grained model for a Cu_3Au system undergoing an order-disorder transition is constructed. The model is characterized by a Ginzburg-Landau Hamiltonian with a three-component order parameter and the symmetry of the Cu_3Au system. The ordering dynamics of this model subjected to a temperature quench are then studied by use of Langevin dynamics. The model is analyzed with a generalization of the recently developed first-principles theory of unstable thermodynamic systems. The theoretical results are in agreement with the observed features in recent growth-kinetic experiments on Cu_3Au.

I. INTRODUCTION

In the past decade, our understanding of growth kinetics[1] problems in relatively simple systems has advanced considerably through simulations on kinetic Ising models[2] and simple Langevin models[3] which are believed to describe some universal features of binary-alloy systems. The most fascinating features observed in both numerical simulations and real experiments on growth-kinetic phenomena are the existence of a dominant time-dependent length—the characteristic domain size $L(t)$ and the scaling behavior of the nonequilibrium structure factor $\tilde{C}(\mathbf{q},t)$ with respect to $L(t)$ at late times. For most systems[1-4] the domain size shows a power-law growth at late times, $L(t)\sim t^n$. Much work in this field has been concentrated on the determination of the growth exponent n. The exponent n has been found to be quite universal[1-4] and depends on only a few factors, such as whether the order parameter is conserved or nonconserved. Attention has been turning to the study of the universal features of the structure factor. Some of the most interesting universal features, such as Porod's law,[5] are very difficult[6] to determine numerically. Recently, Mazenko[7] amd Mazenko, Valls, and Zanetti[8] (MVZ) have developed a first-principles theoretical approach for studying the growth kinetics of simple Langevin equations subjected to a temperature quench. This approach makes possible a more detailed study of the universal features of the structure factor. In this paper, we extend this approach to a richer model that faithfully describes most of the observed growth-kinetic features of a Cu_3Au system undergoing an order-disorder transition.

The theory of Mazenko and MVZ is developed to deal with the problem of separating the dynamics of the two important length scales in the problem, the characteristic domain size $L(t)$ and the equilibrium correlation length ξ. The former characterizes the growth of domains and the latter the fluctuations within a domain. The main physical motivation behind the formalism is the recognition that each field can be decomposed into the sum of a pair of fields. One of these fields is associated with the domain growth and the peak in the structure factor and the other with the fluctuations within an ordered domain. At low temperature T and long time t, the peak contribution to the structure factor is of order unity while the fluctuation contribution is of order T. Here we extend their approach to the case of Langevin equations appropriate to Cu_3Au. This requires the construction, in Sec. II, of a coarse-grained Ginzburg-Landau Hamiltonian characteristic of Cu_3Au. This model involves a three-component order parameter and a nonordering concentration field. The order parameter is nonconserved while the concentration is conserved. We study the Langevin equations of this model subjected to a temperature quench in Sec. III. Thus, by generalizing the theoretical approach of Mazenko, we derive the equation of motion for the ordering components of the order parameter. The analytic and numerical results obtained from an analysis of the resulting equation of motion are given in Sec. IV where they are compared with the observed features in recent growth-kinetic experiments[9,10] on Cu_3Au.

We summarize here the main results of our theory, which agree with experiments. (i) The growth shows distinct physical regimes from early to late times, which can be distinguished by the line shapes of the structure factor. The line shape of the structure factor evolves from Gaussian shape at early times to approximately Lorentzian-squared shape at late stages. (ii) At late times in the coarsening regime, the domain size grows with a power law $L(t)\sim t^{1/2}$. (iii) The peak part of the structure factor of the order parameter exhibits scaling of the form

$$\tilde{C}(\mathbf{q},t)=[L(t)]^d F_{\mathbf{q}}(\mathbf{q}L(t)) \tag{1.1}$$

where $\mathbf{q}$ is the deviation from the superlattice[11] ordering wave vector $\mathbf{Q}$, d is the spatial dimensionality, and the shape function $F_{\mathbf{q}}$, is anisotropic in $\mathbf{q}$ space and has been computed numerically. The anisotropy results from the existence of two different types of domain walls in this system. For the (100) superlattice peak, where $\mathbf{Q}=2\pi(1,0,0)$, the width of longitudinal (parallel to $\mathbf{Q}$) profile is narrower than that of transverse (perpendicular to $\mathbf{Q}$) profile, but both profiles have the same line shape. (iv) The tail of the late stage line shape is shown, both

analytically and numerically, to obey Porod's law[5] [short distance scattering from a sharp interface, $\tilde{C}(\mathbf{q},t) \sim q^{-(d+1)}$ for large q in d dimensions].

II. CONSTRUCTION OF MODEL

The full phase diagram[12,13] for Cu_xAu_{1-x} with any composition of Cu and Au is very rich and complicated. For our purpose of study here, we focus on the fixed concentration with Cu_3Au structure. The Cu_3Au system is the classic example of order-disorder transitions[12-14] and is the most studied experimental[9,10,13,14] system. The disordered phase forms a face-centered-cubic (fcc) crystal with four equivalent sites at (0,0,0), $(\frac{1}{2},\frac{1}{2},0)$, $(\frac{1}{2},0,\frac{1}{2})$, and $(0,\frac{1}{2},\frac{1}{2})$ as shown in Fig. 1, where the lattice constant has been set to one. Each site can be randomly occupied by a Cu atom with a probability $\frac{3}{4}$ and by a Au atom with a probability $\frac{1}{4}$. Below the transition temperature T_c ($\sim 390\,^\circ$C), the system orders in the Cu_3Au crystal structure with one kind of occupation (Au atom) for the site arbitrarily chosen at (0,0,0) and another occupation (Cu atom) at the three equivalent sites $(\frac{1}{2},\frac{1}{2},0)$, $(\frac{1}{2},0,\frac{1}{2})$, and $(0,\frac{1}{2},\frac{1}{2})$. In a perfectly ordered phase, the fcc lattice is filled with alternating all Cu planes and 50% Cu planes. Each Au atom has 12 Cu atoms and no Au atoms as nearest neighbors, and each Cu atom has eight Cu atoms and four Au atoms as nearest neighbors. Since any of the four equivalent sites on the fcc lattice could be the origin for the Cu_3Au structure, there are four types of distinguishable domains.

In the processes of ordering after a temperature quench from a high-temperature disordered state, these four types of domains can coexist with two types of walls,[12,14] as shown in Fig. 2. The two types of walls may be characterized by (1) half-diagonal slip *in* planes perpendicular to the cubic axis [in Fig. 2 the domain on the top is displaced from the one in the center by $\hat{\mathbf{x}}/2+\hat{\mathbf{y}}/2$ in the (001) plane]; and (2) half-diagonal slip *across* planes perpendicular to the cubic axis [in Fig. 2 the domains on the left and right are displaced from the one in the center by $\hat{\mathbf{x}}/2+\hat{\mathbf{y}}/2$ *out of* the (100) and (010) planes, respectively]. Type-1 walls preserve unlike nearest neighbors, while type-2 walls change the number of unlike nearest-neighbor bonds, for sites along the walls. Hence type-1 walls cost less extra energy and are easier to form than type-2 walls.

In discussing the static or dynamic behavior of a system undergoing a phase transition, our first step is to identify the order parameters and to construct a coarse-grained phenomenological Ginzburg-Landau effective Hamiltonian, which is consistent with the symmetry of the system. The fcc lattice can be viewed as four interpenetrating simple cubic sublattices with minimum displacements from the origin: $\mathbf{a}_1=(0,0,0)$, $\mathbf{a}_2=(\frac{1}{2},\frac{1}{2},0)$, $\mathbf{a}_3=(\frac{1}{2},0,\frac{1}{2})$, and $\mathbf{a}_4=(0,\frac{1}{2},\frac{1}{2})$. We denote the occupation on the ith sublattice by $s_i(\mathbf{R})$ ($i=1$, 2, 3, and 4), where $\mathbf{R}$ is a point on sublattice 1, and assign Isinglike occupation numbers

$$s_i(\mathbf{R})=\begin{cases}+1, & \text{if occupied by a Cu atom}\\ -1, & \text{if occupied by a Au atom}\end{cases}. \tag{2.1}$$

The occupation number of Cu atoms is $(1+s)/2$, and that of Au atoms is $(1-s)/2$. The order parameter and the associated Ginzburg-Landau effective Hamiltonian can then be constructed by using the group-theoretical method of Landau and Lifshitz[15-17] for structural phase transitions on the basis of symmetry considerations. According to the Landau-Lifshitz rules, the order parameter has three components, which can be identified as

$$\psi_1(\mathbf{R})=\frac{\psi_0}{2}[\bar{s}_1(\mathbf{R})-\bar{s}_2(\mathbf{R})-\bar{s}_3(\mathbf{R})+\bar{s}_4(\mathbf{R})]\,, \tag{2.2a}$$

$$\psi_2(\mathbf{R})=\frac{\psi_0}{2}[\bar{s}_1(\mathbf{R})-\bar{s}_2(\mathbf{R})+\bar{s}_3(\mathbf{R})-\bar{s}_4(\mathbf{R})]\,, \tag{2.2b}$$

$$\psi_3(\mathbf{R})=\frac{\psi_0}{2}[\bar{s}_1(\mathbf{R})+\bar{s}_2(\mathbf{R})-\bar{s}_3(\mathbf{R})-\bar{s}_4(\mathbf{R})]\,, \tag{2.2c}$$

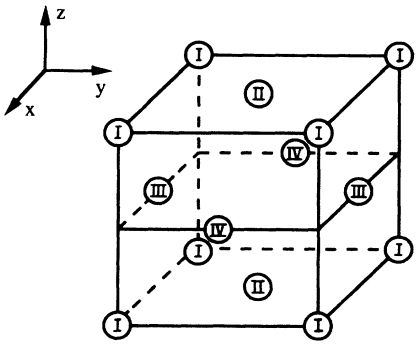

FIG. 1. The unit cell of the face-centered-cubic lattice. The lattice constant is taken to be unity. I, II, III, and IV are the four equivalent simple cubic sublattices.

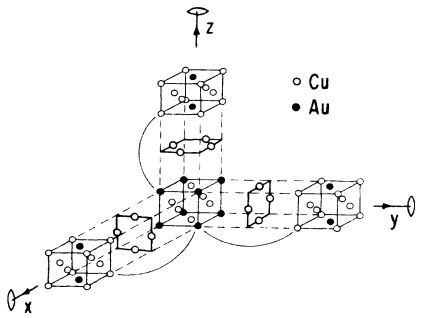

FIG. 2. The domain at the origin is specified by the state $(-1,-1,-1,0)\psi_0$, and the other three on the three axes are specified by the state $(1,1,-1,0)\psi_0$. Assume these domains are separated by an all Cu layer in between. This layer can be viewed as part of the domain on the top or part of the domain at the center, but not part of the domains on the left and right. The dashed lines mean the elongated lattice spacing to show clearly the intermediate all-Cu layer.

where $\psi_0>0$ is the magnitude of the equilibrium average value of the order parameter and $\bar{s}_i$ means the average[18] over four equivalent sites of $\mathbf{a}_i$ with respect to the lattice point $\mathbf{R}$. For the vector $\mathbf{a}_i$, its four equivalent vectors are denoted by $\mathbf{a}_{ij}$ ($j=1$, 2, 3, and 4) and are listed in Table I as the ith row. For example, the sites with the displacements $(\frac{1}{2},\frac{1}{2},0)$, $(-\frac{1}{2},\frac{1}{2},0)$, $(\frac{1}{2},-\frac{1}{2},0)$, and $(-\frac{1}{2},-\frac{1}{2},0)$ from the lattice point $\mathbf{R}$ are equivalent. Since the total number of Cu and Au atoms is conserved there is a conserved "concentration,"

$$\Psi=\frac{\psi_0}{2}[\bar{s}_1(\mathbf{R})+\bar{s}_2(\mathbf{R})+\bar{s}_3(\mathbf{R})+\bar{s}_4(\mathbf{R})-2] . \quad (2.2d)$$

Note that ψ_α ($\alpha=1$, 2, and 3) and Ψ are defined on a simple cubic lattice and are linearly independent. In the disordered phase, $\bar{s}_i=\frac{1}{2}$, and (2.2a)–(2.2d) give $\psi_\alpha=\Psi=0$. In the ordered phase, depending on the positions of the Au atoms, there are four ordered states that are specified by the ψ_α and Ψ and listed in Table II. If the symmetry of states is unbroken as in the ordering processes, the four states are equally likely to coexist. From Table II, we immediately obtain

$$\langle\psi_\alpha\rangle=0 , \quad (2.3a)$$

$$\langle\psi_\alpha\psi_\beta\rangle=0 \quad \text{for } \alpha\neq\beta , \quad (2.3b)$$

$$\langle\Psi\rangle=0 , \quad (2.3c)$$

$$\langle\psi_\alpha\Psi\rangle=0 , \quad (2.3d)$$

where the average is over the four ordered states. We also have the relation, for any ordered state,

$$\psi_1\psi_2\psi_3=-\psi_0^3<0 . \quad (2.4)$$

The coarse-grained Ginzburg-Landau potential, which can be constructed from the three components of the order parameter and the conserved concentration with corresponding symmetry, is given by

$$U=\frac{r}{2}\sum_\beta\psi_\beta^2+w\psi_1\psi_2\psi_3 + \frac{v}{4}\sum_\beta\psi_\beta^4+\frac{u}{4}\left[\sum_\beta\psi_\beta^2\right]^2+\frac{r'}{2}\Psi^2 , \quad (2.5)$$

where the order parameter ψ_β and concentration Ψ are treated as continuous fields in the sense of coarse graining and β runs from 1 to 3. Let us now consider the mean-field theory analysis of (2.5). By minimizing U with respect to ψ_α and Ψ, we can easily determine the signs of the parameters for (2.5) to be appropriate for a description of Cu_3Au. As usual we take $r=r_0(T-T_c)$ for T near T_c, where $r_0>0$, and w, v, u, and r' must all be positive. With these choices the potential produces the same equilibrium disordered and ordered states as those listed in Table II with ψ_0 satisfying the following equation of state:

$$(3u+v)\psi_0^2-w\psi_0+r=0 . \quad (2.6)$$

or,

$$\psi_0=\frac{1}{2(3u+v)}\{w+[w^2-4r(3u+v)]^{1/2}\} . \quad (2.7)$$

Note that the cubic term in (2.5), $w\psi_1\psi_2\psi_3$, distinguishes Cu_3Au from $CuAu_3$. If $w<0$, the ordered states of the potential would correspond to $CuAu_3$ instead of the Cu_3Au system. If $w=0$, then Cu_3Au and $CuAu_3$ states are indistinguishable and the ordered-state degeneracy becomes eight. Thus the choice $w>0$ picks four ordered states out of a possible eight states. It can be easily shown that, due to the existence of the cubic term in (2.5), the ordering transition of this model is first order, which agrees with the experimental[13] observation of Cu_3Au system.

We now consider the extra energy cost due to the presence of domain walls. The obvious contributions of extra energy cost from the walls are the isotropic gradient[19] terms

$$\frac{c_1}{2}\sum_\beta(\nabla\psi_\beta)^2+\frac{c_1'}{2}(\nabla\Psi)^2 , \quad (2.8)$$

where β runs from 1 to 3. Let us now calculate the energy cost for the domain walls in Fig. 2 using (2.28). The domain located at the origin corresponds to the state $(-1,-1,-1,0)\psi_0$, while those on the three axes correspond to the state $(1,1-1,0)\psi_0$. From (2.28) and Table II and using lattice versions of the gradient terms, we can easily find that the extra energy cost due to the walls is $4c_1\psi_0^2$ per unit wall area, which is the same for both types of domain walls. Thus we need another anisotropic gradient term to distinguish type-2 walls from type-1 walls. Looking at Fig. 2 and the two states more carefully, we see that the type of wall separating the two states (domains) depends on the relative orientations of the two states (domains). For the two states $(-1,-1,-1,0)\psi_0$ and $(1,1,-1,0)\psi_0$ the third component of the order pa-

TABLE I. The fcc lattice can be viewed as four simple cubic sublattices with minimum displacements $\mathbf{a}_{i1}$ ($i=1$, 2, 3, and 4), given by the first column, from the origin. For each given i, there are four equivalent vectors $\mathbf{a}_{ij}$ ($j=1$, 2, 3, and 4), given by the ith row.

(0,0,0)	(0,0,0)	(0,0,0)	(0,0,0)
$(\frac{1}{2},\frac{1}{2},0)$	$(-\frac{1}{2},\frac{1}{2},0)$	$(-\frac{1}{2},-\frac{1}{2},0)$	$(\frac{1}{2},-\frac{1}{2},0)$
$(\frac{1}{2},0,\frac{1}{2})$	$(\frac{1}{2},0,-\frac{1}{2})$	$(-\frac{1}{2},0,-\frac{1}{2})$	$(-\frac{1}{2},0,\frac{1}{2})$
$(0,\frac{1}{2},\frac{1}{2})$	$(0,-\frac{1}{2},\frac{1}{2})$	$(0,-\frac{1}{2},-\frac{1}{2})$	$(0,\frac{1}{2},-\frac{1}{2})$

TABLE II. Depending on the position of Au atoms on the fcc lattice, there are four equilibrium ordered states. The numbers in the first column indicate the position of the Au atom in Fig. 1.

	(s_1,s_2,s_3,s_4)	$(\psi_1,\psi_2,\psi_3,\Psi)$
I	$(-1,1,1,1)$	$(-1,-1,-1,0)\psi_0$
II	$(1,-1,1,1)$	$(1,1,-1,0)\psi_0$
III	$(1,1,-1,1)$	$(1,-1,1,0)\psi_0$
IV	$(1,1,1,-1)$	$(-1,1,1,0)\psi_0$

rameter has the same sign for both states while the first and second components flip signs. Hence, if we introduce the anisotropic gradient term

$$\frac{c_2}{2}\sum_{\beta}(\nabla_\beta\psi_\beta)^2 , \tag{2.9}$$

we immediately see that this term vanishes for type-1 walls (separating the top domain from the center domain in Fig. 2), but costs extra energy, $2c_2\psi_0^2$, for type-2 walls [separating the left (right) domain from the center domain in Fig. 2]. Thus for $c_2>0$ the total extra energy cost for type-2 walls is $(4c_1+2c_2)\psi_0^2$ per unit wall area, while that for type-1 walls is $4c_1\psi_0^2$. For later convenience, we define the anisotropy parameter $a=c_2/c_1$. The ratio of extra energy cost of type-2 walls to type-1 walls is then $1+a/2$. The above arguments hold for the walls between any two ordered states.

Putting all the terms together, the total coarse-grained Ginzburg-Landau effective Hamiltonian can be written, in the continuum[19,20] limit, as

$$\begin{aligned}H=\int d^dR\Bigg[&\frac{c_1}{2}\left[\sum_\beta(\nabla\psi_\beta)^2+a\sum_\beta(\nabla_\beta\psi_\beta)^2\right]\\&+\frac{r}{2}\sum_\beta\psi_\beta^2+w\psi_1\psi_2\psi_3\\&+\frac{v}{4}\sum_\beta\psi_\beta^4+\frac{u}{4}\left[\sum_\beta\psi_\beta^2\right]^2\\&+\frac{c_1'}{2}(\nabla\Psi)^2+\frac{r'}{2}\Psi^2\Bigg] .\end{aligned} \tag{2.10}$$

Thus the problem of Cu_3Au on the fcc lattice is now described by the Ginzburg-Landau effective Hamiltonian (2.10) with a three-component order parameter and a concentration field defined on the simple cubic lattice. The Hamiltonian (2.10) differs from the usual $O(3)$ symmetric model[21] in several aspects: (i) the v term adds the cubic symmetry of the lattice; (ii) the w term distinguishes Cu_3Au from $CuAu_3$ and makes the equilibrium transition first order rather than second order, as in the scalar order parameter case; and (iii) the gradient term with coefficient a introduces anisotropy and makes type-2 walls cost more extra energy than type-1 walls. The portion of the Hamiltonian (2.10) dependent on ψ becomes the Ginzburg-Landau theory of the four-state Potts model[22] if the anisotropic gradient term is removed ($a=0$). This term breaks the Potts symmetry (i.e., invariance under permutations of the ordered states) by introducing a coupling between the lattice coordinates and the order parameter. Thus, this four-state model is particular to three-dimensional systems with Cu_3Au structure while the four-state Potts model may of course be generalized to any spatial dimension.

III. DYNAMICS AND METHODS

The dynamics of the order parameter ψ_α associated with the Ginzburg-Landau Hamiltonian (2.10) are assumed to be governed by the Langevin equation,

$$\frac{\partial\psi_\alpha}{\partial t}=-\Gamma_0\frac{\delta H}{\delta\psi_\alpha}+\eta_\alpha , \tag{3.1}$$

i.e.,

$$\begin{aligned}\frac{\partial\psi_\alpha}{\partial t}=-\Gamma_0\Big[&-c_1(\nabla^2+a\nabla_\alpha^2)\psi_\alpha+r\psi_\alpha\\&+w\psi_{\alpha-1}\psi_{\alpha+1}+v\psi_\alpha^3+u\left[\sum_\beta\psi_\beta^2\right]\psi_\alpha\Big]+\eta_\alpha ,\end{aligned} \tag{3.2}$$

where α and β run from 1 to 3. In (3.2), $\Gamma_0>0$ is just a constant relaxation rate in the case of nonconserved order parameter. η_α appearing in (3.2) is the Gaussian noise and satisfies the fluctuation-dissipation relation

$$\langle\eta_\alpha(\mathbf{R},t)\eta_\beta(\mathbf{R}',t')\rangle=2T\Gamma_0\delta_{\alpha\beta}\delta(\mathbf{R}-\mathbf{R}')\delta(t-t') , \tag{3.3}$$

where T is the final temperature and Boltzmann's constant k_B is taken to be unity. The concentration field Ψ is conserved and nonordering, and satisfies a diffusion equation. It can be shown that the Ψ field relaxes exponentially with time for the wave numbers near the superlattice peak and does not play any role in the ordering processes. Hence it is omitted in the remainder of this paper.

We are here interested in the ordering dynamics of Eq. (3.2), which characterizes the growth of domains of the new ordered phases. Specifically, we consider the case where the system is initially in a disordered equilibrium state at some high temperature T_I and at time $t=t_0$ is quenched to some low temperature T well below its ordering temperature T_c. The initial probability distribution governing ψ_α at time t_0 is assumed to be Gaussian and the initial correlation is given by

$$\langle\psi_\alpha(\mathbf{R},t_0)\psi_\beta(\mathbf{R}',t_0)\rangle=\varepsilon_I\delta_{\alpha\beta}\delta(\mathbf{R}-\mathbf{R}') , \tag{3.4}$$

where ε_I is a measure of the initial temperature. The theoretical treatment of the quench problem associated with Eq. (3.2) follows the parallel development in MVZ and Mazenko with ψ now a three-component vector. We leave out the detailed formal development and just briefly mention the major steps.

The equation of motion (3.2) can be reformulated into a functional integral representation.[7,8] The dynamics of the ψ fields can be fully described in terms of a probability distribution $P[\psi]$. The key point in the development is the introduction of auxiliary fields $m_\alpha(\mathbf{x},t)$, which govern the ordering components of the fields ψ_α. This is done by first expanding the functional space

$$P[\psi]\rightarrow P[\psi,m]=P[\psi]P[m] ,$$

where $P[m]$ is a properly normalized probability distribution governing the m fields. Next, decompose the original fields into the sum of the ordering and fluctuating parts via

$$\psi_\alpha(\mathbf{R},t)=\sigma_\alpha(\mathbf{R},t)+\phi_\alpha(\mathbf{R},t) , \tag{3.5}$$

where $\{\sigma_\alpha\}$ are functionals of the fields $\{m_\alpha\}$ and will be specified later. As discussed in MVZ, we would expect

the peak or ordering variables $\sigma_\alpha(\mathbf{R},t)$ to become associated with the growth of domains and $\phi_\alpha(\mathbf{R},t)$ with the fluctuations within a domain.

For our purpose here, we focus on the dynamics of the ordering peak contribution. Following Mazenko, this can be specified primarily by two requirements: (i) $P[m]$ is a Gaussian distribution and (ii) the variance of $P[m]$ is determined by requiring

$$\left\langle \sigma_\alpha(2)\left\{\frac{\partial\sigma_\alpha(1)}{\partial t_1}+\Gamma_0\left[-c_1(\nabla^2+a\nabla_\alpha^2)\sigma_\alpha(1)+r\sigma_\alpha(1)+w\sigma_{\alpha-1}(1)\sigma_{\alpha+1}(1)+v\sigma_\alpha^3(1)+u\left[\sum_\beta\sigma_\beta^2(1)\right]\sigma_\alpha(1)\right]\right\}\right\rangle = \langle\sigma_\alpha(2)\sigma_\alpha(1)\delta(t_1-t_0)\rangle\ , \quad (3.6)$$

where the average is over $P[m]$, $\sigma_\alpha(1)=\sigma_\alpha(\mathbf{R}_1,t_1)$, and α and β run from 1 to 3 and cyclic permutations. The right-hand side of (3.6) is just the initial condition. The cross-correlation functions $\langle\sigma_\alpha(1)\sigma_\beta(2)\rangle$ $(\alpha\neq\beta)$ can be shown to vanish. The first requirement is motivated by simplicity. The second requirement demands that the correlation function of σ_α satisfies the noiseless equation of motion (3.2) on average and ensures that the coupling between σ_α and ϕ_α variables vanishes as $t\to\infty$. As discussed in MVZ, the coupling between σ_α and ϕ_α can be treated using perturbation theory which is valid for low temperatures. The analysis follows that in MVZ rather closely, and the upshot is that the coupling between σ_α and ϕ_α contributes some early time transient, but does not change the qualitative behavior of the σ_α field. We must also specify the initial conditions satisfied by the σ_α and m_α fields. As pointed out in MVZ, the behavior of the full correlation function is very insensitive to the choice of initial conditions for σ_α. It is therefore reasonable to choose σ_α to satisfy the same initial conditions as ψ_α given by (3.4).

Before proceeding to carry out the average over $P[m]$ implied in (3.6), we must specify the functional $\sigma_\alpha=\sigma_\alpha(m_\beta)$. Since σ_α represents the growth of domains, we would expect the functional to show some kind of domain structure. In the recent approach by Mazenko for a scalar order parameter model, σ is related to m by a nonlinear functional

$$\sigma(\mathbf{R},t)=\psi_0\tanh m(\mathbf{R},t)\ , \quad (3.7)$$

where ψ_0 is the equilibrium average value of the order parameter. The choice of Eq. (3.7) has a well-defined physical meaning: $\psi_0\tanh(z/\xi)$, where ξ is correlation length ($\sim$interfacial width), is nothing but the one-dimensional kink solution for the scalar ψ^4 Hamiltonian. Thus, Eq. (3.7) implies that σ represents randomly distributed domain walls located at $m=0$ and gives the correct interfacial profile. The width of the interface is governed by $P[m]$.

For our model with a three-component order parameter, if we could find the static kink solutions to the Hamiltonian (2.10), they might be used to construct the appropriate functional $\sigma_\alpha(m_\beta)$. Unfortunately, we do not know these kink solutions. We might hope to simply choose (3.7) as the functional for our model. This is not acceptable since it would lead to $\langle\sigma_1\sigma_2\sigma_3\rangle\equiv0$ for average over the Gaussian distribution $P[m]$ and would not reflect the domain structure of our model. However, we can construct a functional that can approximately represent or mimic very well the domain structure of our model, especially at long times.

From the equilibrium ordered-state solutions in Table II and the relation (2.4), we immediately see that for any one of the four ordered states the product of the three components of the order parameter is negative definite. Furthermore, when one goes from one ordered state to another, two of the three components change sign and the other retains the same sign. It can be easily seen that the following choice of σ_α satisfies the above constraints.

$$\sigma_1(\mathbf{R})=-\psi_0\tanh m_2(\mathbf{R})\tanh m_3(\mathbf{R})\ , \quad (3.8a)$$

$$\sigma_2(\mathbf{R})=-\psi_0\tanh m_3(\mathbf{R})\tanh m_1(\mathbf{R})\ , \quad (3.8b)$$

$$\sigma_3(\mathbf{R})=-\psi_0\tanh m_1(\mathbf{R})\tanh m_2(\mathbf{R})\ , \quad (3.8c)$$

or, in short,

$$\sigma_\alpha(\mathbf{R})=-\psi_0\tanh m_{\alpha-1}(\mathbf{R})\tanh m_{\alpha+1}(\mathbf{R})\ . \quad (3.9)$$

where $\alpha=1$, 2, 3, and cyclic permutations. It is obvious that (3.9) reproduces the correct equilibrium ordered states, listed in Table II, as $m_\alpha\to\pm\infty$. Thus, Eq. (3.9) implies that σ_α represents randomly distributed domain walls and should mimic the interfacial profile of our model. For the moment let us choose Eq. (3.9) as the acceptable functional, which relates $\{\sigma_\alpha\}$ to $\{m_\alpha\}$.

We now can carry out the Gaussian average over $P[m]$ implied in Eq. (3.6). Since at any finite time of the ordering processes any of the four ordered states are equally favored, we must have

$$\langle\sigma_\alpha\rangle=-\psi_0\langle\tanh m_{\alpha-1}\tanh m_{\alpha+1}\rangle\equiv0\ . \quad (3.10)$$

This requires that, for Gaussian average,

$$\langle m_\alpha(1)m_\beta(2)\rangle=\delta_{\alpha\beta}\langle m_\alpha(1)m_\alpha(2)\rangle\ . \quad (3.11)$$

This means the Gaussian probability distribution must be diagonal,

$$P[m]=P[m_1]P[m_2]P[m_3]\ . \quad (3.12)$$

Using (3.9), Eq. (3.6) can now be expressed in terms of $\{m_\alpha\}$. For example,

$$\langle\sigma_\alpha(1)\sigma_\alpha(2)\rangle=\psi_0^2\langle\tanh m_{\alpha-1}(1)\tanh m_{\alpha-1}(2)\rangle\langle\tanh m_{\alpha+1}(1)\tanh m_{\alpha+1}(2)\rangle\ . \quad (3.13)$$

The multipoint correlation functions can be expressed in the same way. For later convenience, we define the following quantities:

$$T_\alpha(12)=\langle \tanh m_\alpha(1)\tanh m_\alpha(2)\rangle \ , \tag{3.14}$$

$$K_\alpha(12)=\left\langle \frac{\tanh m_\alpha(1)}{\cosh^2 m_\alpha(1)}\tanh m_\alpha(2)\right\rangle \ , \tag{3.15}$$

$$S(t_1)\equiv S_\alpha(t_1)=T_\alpha(11)\equiv 1-\left\langle \frac{1}{\cosh^2 m_\alpha(1)}\right\rangle \ , \tag{3.16}$$

$$C^0_\alpha(12)=\langle m_\alpha(1)m_\alpha(2)\rangle \ , \tag{3.17}$$

$$S_0(t_1)\equiv S^0_\alpha(t_1)=C^0_\alpha(11) \ . \tag{3.18}$$

In (3.16) and (3.18), the quantities for $1=2$ are independent of the index α due to permutation symmetry and spatial translational invariance. Thus the normalized correlation function can be expressed as

$$\begin{aligned} C_\alpha(12)&=\psi_0^{-2}\langle \sigma_\alpha(1)\sigma_\alpha(2)\rangle \\ &=T_{\alpha-1}(12)T_{\alpha+1}(12) \ . \end{aligned} \tag{3.19}$$

Equation (3.19) can be inverted to give

$$T_\alpha(12)=\left[\frac{C_{\alpha-1}(12)C_{\alpha+1}(12)}{C_\alpha(12)}\right]^{1/2} \ . \tag{3.20}$$

Using (3.9) and assuming spatial translational invariance, the equation of motion (3.6) can be rewritten as, at equal times $t_1=t_2=t$,

$$\begin{aligned} &\left[\frac{\partial}{\partial t}+2\Gamma_0\{-c_1(\nabla^2+a\nabla^2_\alpha)+(w\psi_0-2u\psi_0^2)[1-S(t)]\}\right]T_{\alpha-1}(\mathbf{R},t)T_{\alpha+1}(\mathbf{R},t) \\ &\quad -2\Gamma_0\psi_0^2[v+u+uS(t)][T_{\alpha-1}(\mathbf{R},t)K_{\alpha+1}(\mathbf{R},t)+T_{\alpha+1}(\mathbf{R},t)K_{\alpha-1}(\mathbf{R},t)] \\ &\quad +2\Gamma_0(v+u)\psi_0^2K_{\alpha-1}(\mathbf{R},t)K_{\alpha+1}(\mathbf{R},t)=0 \ , \end{aligned} \tag{3.21}$$

where we have dropped the term with δ function at $t=t_0$ and treat the quench problem as an initial value problem. In Eq. (3.21), $T_\alpha(\mathbf{R},t)$, $K_\alpha(\mathbf{R},t)$, and $S(t)$ are defined by (3.14), (3.15), and (3.16) and are related to $C^0_\alpha(\mathbf{R},t)$ and $S_0(t)$ in a rather complicated fashion as shown below.

Using the integral representation

$$\tanh m=\int_0^{+\infty}\frac{dz\,\sin(mz)}{\sinh(\pi z/2)} \ , \tag{3.22}$$

we can write

$$T_\alpha(12)=\int_0^{+\infty}\frac{dz_1}{\sinh(\pi z_1/2)}\int_0^{+\infty}\frac{dz_2}{\sinh(\pi z_2/2)}\langle \sin[m_\alpha(1)z_1]\sin[m_\alpha(2)z_2]\rangle \ . \tag{3.23}$$

Recall the identity

$$\sin(mz)=\sum_{\alpha=\pm 1}\frac{\alpha}{2i}e^{i\alpha mz} \ ,$$

and for Gaussian average over the m variables

$$\left\langle \exp\left[\int d1\,h(1)m(1)\right]\right\rangle=\exp\left[\tfrac{1}{2}\int d\bar{1}\,d\bar{2}\,C^0(\bar{1}\bar{2})h(\bar{1})h(\bar{2})\right] \ , \tag{3.24}$$

where $h(1)$ can be any function and $C^0(12)=\langle m(1)m(2)\rangle$. Then $T_\alpha(\mathbf{R},t)$, given by (3.23), can be evaluated in terms of $C^0_\alpha(\mathbf{R},t)$,

$$T_\alpha(\mathbf{R},t)=\int_0^{+\infty}\frac{dz_1}{\sinh(\pi z_1/2)}\int_0^{+\infty}\frac{dz_2}{\sinh(\pi z_2/2)}\exp[-\tfrac{1}{2}S_0(t)(z_1^2+z_2^2)]\sinh[z_1z_2C^0_\alpha(\mathbf{R},t)] \ , \tag{3.25}$$

$$=\int_{-\infty}^{+\infty}\frac{dx_1}{\sqrt{2\pi}}\frac{dx_2}{\sqrt{2\pi}}\exp[-\tfrac{1}{2}(x_1^2+x_2^2)]\tanh(x_2b_{\alpha+}-x_1b_{\alpha-})\tanh(x_2b_{\alpha-}+x_1b_{\alpha+}) \ , \tag{3.26}$$

where $b^2_{\alpha\pm}=\frac{1}{2}[S_0(t)\pm C^0_\alpha(\mathbf{R},t)]$ and use has been made of spatial translational invariance and $t_1=t_2=t$. The second form (3.26), follows from using the identity $\int_{-\infty}^{+\infty}(dx/\sqrt{2\pi})\exp[-\frac{1}{2}x^2+ixy]=\exp[-\frac{1}{2}y^2]$ twice. Likewise, using the integral representation

$$\frac{\tanh m}{\cosh^2 m}=-\frac{1}{2}\frac{d^2\tanh m}{dm^2}=\frac{1}{2}\int_0^{+\infty}\frac{dz\,z^2\sin(mz)}{\sinh(\pi z/2)} \tag{3.27}$$

we immediately obtain,

$$K_\alpha(\mathbf{R},t)=-\frac{1}{2}\frac{\partial T_\alpha(\mathbf{R},t)}{\partial S_0(t)}\bigg|_{C_\alpha^0(\mathbf{R},t)}, \tag{3.28}$$

where $T_\alpha(\mathbf{R},t)$ is given by (3.25) or (3.26).

Before continuing with the complicated equation of motion, (3.21), it is profitable to briefly discuss the basic nature of the expected solution in the long-time limit. From (3.16) we have

$$\begin{aligned} S(t)&=\langle\tanh^2 m_\alpha(t)\rangle=1-\left\langle\frac{1}{\cosh^2 m_\alpha(t)}\right\rangle \\ &=1-\int\frac{dx}{\sqrt{2\pi}}\frac{e^{-(1/2)x^2}}{\cosh^2[x\sqrt{S_0(t)}]} \\ &=1-\left[\frac{2}{\pi S_0(t)}\right]^{1/2}+O(S_0^{-3/2}) \end{aligned} \tag{3.29}$$

for large $S_0(t)$. In the limit $t\to\infty$, the system approaches equilibrium and we expect $S(t)\to 1$, which implies that $S_0(\infty)\to\infty$. Thus $S_0(t)$ grows with time without bound and must be related to the domain size $L(t)$. Physically we expect the interfaces to become very sharp at long times. Assuming[23] that the domains with size L are separated by interfaces with width ξ, then the total volume is $(L+\xi)^d$ in d dimensions. The volume over which the order parameter is nonzero is L^d. Therefore we can estimate

$$S^2=\psi_0^{-2}\langle\psi_\alpha^2\rangle\sim\left[\frac{L}{L+\xi}\right]^d=1-\frac{\xi d}{L}+O\left[\frac{1}{L^2}\right], \tag{3.30}$$

and

$$S=1-\frac{\xi d}{2L}+O\left[\frac{1}{L^2}\right]. \tag{3.31}$$

Comparing (3.31) with (3.29), we can identify $S_0\sim L^2$ and $1-S\sim O(1/L)$. For the convenience of later discussion, we define

$$L^2(t)\equiv\frac{2}{[1-S(t)]^2}=\pi S_0(t), \tag{3.32}$$

where the second identity holds to leading order in S_0 as follows from (3.29).

We now want to see if the equation of motion, (3.21), leads to the expected long-time results in the sharp interface limit. In the long-time limit, where S_0 is large [and $C_\alpha^0(\mathbf{R})/S_0$ is held fixed], (3.21) can be simplified considerably. For example (for $\mathbf{R}\neq\mathbf{0}$), in the sharp interface limit, (3.26) can be replaced by

$$T_\alpha(\mathbf{R},t)=\int_{-\infty}^{+\infty}\frac{dx_1}{\sqrt{2\pi}}\frac{dx_2}{\sqrt{2\pi}}e^{-(1/2)(x_1^2+x_2^2)}\operatorname{sgn}(x_2b_{\alpha+}-x_1b_{\alpha-})\operatorname{sgn}(x_2b_{\alpha-}+x_1b_{\alpha+}). \tag{3.33}$$

Equation (3.33) can be integrated to obtain

$$T_\alpha(\mathbf{R},t)=1-\frac{4}{\pi}\tan^{-1}\left[\frac{S_0-C_\alpha^0(\mathbf{R},t)}{S_0+C_\alpha^0(\mathbf{R},t)}\right]^{1/2} \tag{3.34}$$

which can be inverted to give

$$\frac{C_\alpha^0(\mathbf{R},t)}{S_0}=\sin\left[\frac{\pi}{2}T_\alpha(\mathbf{R},t)\right]. \tag{3.35}$$

Using (3.28) and (3.35) in this limit, we can write

$$K_\alpha(\mathbf{R},t)=\frac{1}{\pi S_0}\tan\left[\frac{\pi}{2}T_\alpha(\mathbf{R},t)\right]. \tag{3.36}$$

Inserting (3.36) into (3.21) and using (3.32), for $S\sim 1$, we obtain the equation of motion

$$\begin{aligned} &\left[\frac{\partial}{\partial t}-2\Gamma_0\{c_1(\nabla^2+a\nabla_\alpha^2)+(2u\psi_0^2-w\psi_0)[1-S(t)]\}\right]T_{\alpha-1}(\mathbf{R},t)T_{\alpha+1}(\mathbf{R},t)-\Gamma_0\psi_0^2\{(v+2u)[1-S(t)]^2 \\ &\quad+u[1-S(t)]^3\}\left[T_{\alpha-1}(\mathbf{R},t)\tan\left[\frac{\pi}{2}T_{\alpha+1}(\mathbf{R},t)\right]+T_{\alpha+1}(\mathbf{R},t)\tan\left[\frac{\pi}{2}T_{\alpha-1}(\mathbf{R},t)\right]\right] \\ &\quad+\frac{\Gamma_0}{2}\psi_0^2(v+u)[1-S(t)]^4\tan\left[\frac{\pi}{2}T_{\alpha-1}(\mathbf{R},t)\right]\tan\left[\frac{\pi}{2}T_{\alpha+1}(\mathbf{R},t)\right]=0. \end{aligned} \tag{3.37}$$

It is one of the most fascinating features associated with the growth-kinetic phenomena that the long-time theory satisfies scaling. Let us analyze (3.37) assuming that all the lengths are scaled by a factor of L. ∇^2, for example, contributes a factor of $1/L^2$. At long times, the term proportional to $[1-S(t)]$ dominates and those proportional to $[1-S(t)]^n$ ($n=2,3,4$) can be neglected. Equation (3.37) is then linear. Thus for scaling to hold, we must have $1-S(t)\sim O(1/L^2)$, which contradicts the previous sharp interface argument that $1-S(t)\sim O(1/L)$. Furthermore, the coefficient of the $[1-S(t)]$ term, $2u\psi_0^2-w\psi_0$, does not have a definitive sign. Its sign depends on the values of parameters u and w. Also, as discussed in Mazenko, this linear equation does not lead to Porod's law.

Since the functional (3.9) does not lead to the required scaling in the sharp interface limit, we need to look for a better approximation than (3.9) near the interface ($m_\alpha \approx 0$). Suppose we can find a functional σ_α such that the term proportional to $[1-S(t)]$ in (3.37) vanishes and the term proportional to $[1-S(t)]^2$ in (3.37) dominates at long times. Then a scaling analysis leads to $[1-S(t)]^2\sim O(1/L^2)$, i.e., $1-S(t)\sim O(1/L)$, which agrees with the sharp interface arguments. Guided by the above idea, we have found that we may choose σ_α to be of the general form

$$\sigma_\alpha(\mathbf{R},t)=-\psi_0 \tanh m_{\alpha-1}\tanh m_{\alpha+1}[1+\Theta(m_\alpha)] , \tag{3.38}$$

where $\Theta(m_\alpha)$ must be an even function of m_α and vanishes as $m_\alpha\to\pm\infty$ for (3.38) to reproduce the correct ordered states. In particular, we will choose[24]

$$\Theta(m_\alpha)=\frac{A_1}{\cosh^2 m_\alpha}+\frac{A_2\tanh^2 m_\alpha}{\cosh^2 m_\alpha}+\frac{A_3\tanh^4 m_\alpha}{\cosh^2 m_\alpha} , \tag{3.39}$$

where A_1, A_2, and A_3 are constants to be determined. As discussed in detail in Appendix A, the term proportional to $[1-S(t)]$ is cancelled by the correction term with the proper choice of the A_i's. The equation of motion, (3.6), can then be rewritten, to order $O(1/L^2)$ and at equal times $t_1=t_2=t$, as

$$\left[\frac{\partial}{\partial t}-2\Gamma_0 c_1(\nabla^2+a\nabla_\alpha^2)\right]T_{\alpha-1}(\mathbf{R},t)T_{\alpha+1}(\mathbf{R},t)-2\Gamma_0 B[T_{\alpha-1}(\mathbf{R},t)K_{\alpha+1}(\mathbf{R},t)+T_{\alpha+1}(\mathbf{R},t)K_{\alpha-1}(\mathbf{R},t)]=0 , \tag{3.40}$$

where $B>0$ and is given by (A7) in Appendix A. Since $O(1/L^3)$ and higher-order terms are neglected in (3.40), only the dominant nonlinear contributions are taken into account. It becomes quantitatively exact in the interesting long-time scaling regime.

For the convenience of later discussion, we rescale Eq. (3.40) into dimensionless form. Let

$$t\to\frac{t}{2\Gamma_0 B} \tag{3.41a}$$

and

$$\mathbf{R}\to\sqrt{(c_1/B)}\mathbf{R} . \tag{3.41b}$$

The dimensionless form of (3.40) is then given by

$$\left[\frac{\partial}{\partial t}-(\nabla^2+a\nabla_\alpha^2)\right]T_{\alpha-1}(\mathbf{R},t)T_{\alpha+1}(\mathbf{R},t)-[T_{\alpha-1}(\mathbf{R},t)K_{\alpha+1}(\mathbf{R},t)+T_{\alpha+1}(\mathbf{R},t)K_{\alpha-1}(\mathbf{R},t)]=0 . \tag{3.42}$$

Note that (3.42) depends only on the anisotropy parameter a.

Inserting (3.36) into (3.42) and using (3.32), we obtain the dimensionless equation of motion in the sharp interface limit

$$\left[\frac{\partial}{\partial t}-(\nabla^2+a\nabla_\alpha^2)\right]T_{\alpha-1}(\mathbf{R},t)T_{\alpha+1}(\mathbf{R},t) -\tfrac{1}{2}[1-S(t)]^2\left[T_{\alpha-1}(\mathbf{R},t)\tan\left[\frac{\pi}{2}T_{\alpha+1}(\mathbf{R},t)\right]+T_{\alpha+1}(\mathbf{R},t)\tan\left[\frac{\pi}{2}T_{\alpha-1}(\mathbf{R},t)\right]\right]=0 . \tag{3.43}$$

Recalling (3.20), Eq. (3.43) can also be rewritten in terms of $C_\alpha(\mathbf{R},t)$. It is obvious that the scaling analysis now gives $1-S(t)\sim O(1/L)$, which is in agreement with the sharp interface arguments. As will be shown in Sec. IV, the nonlinear scaling equation, (3.43), leads to Porod's law.

IV. RESULTS AND DISCUSSIONS

In this section, we present the results obtained from solving the equations of motion, in the sharp interface limit, (3.43). Let us first look at the relationship among the correlation functions defined by (3.19): $C_1(\mathbf{R},t)$,

$C_2(\mathbf{R},t)$, and $C_3(\mathbf{R},t)$. From the equation of motion (3.42), we see that the spatial anisotropy of $C_\alpha(\mathbf{R},t)$ is controlled by the parameter a. If $a=0$, $C_\alpha(\mathbf{R})$ is symmetric among the spatial variables R_1, R_2, and R_3 and $C_1(\mathbf{R})=C_2(\mathbf{R})=C_3(\mathbf{R})$. For $a\neq 0$, using (3.19), (3.20), (3.28), and (3.42), we can show that the correlation function $C_\alpha(\mathbf{R})$ is symmetric between the spatial variables $R_{\alpha-1}$ and $R_{\alpha+1}$ and can be written as

$$C_\alpha(\mathbf{R},t)\equiv C(R_\alpha;R_{\alpha-1},R_{\alpha+1},t)\ , \tag{4.1}$$

where C stands for the correlation function which is symmetric between the second and third spatial variables. Equation (4.1) implies that the three correlation functions, $C_1(\mathbf{R})$, $C_2(\mathbf{R})$, and $C_3(\mathbf{R})$, are equivalent. Taking the Fourier transform of (4.1), we obtain the structure factor

$$\tilde{C}_\alpha(\mathbf{q},t)\equiv \tilde{C}(q_\alpha;q_{\alpha-1},q_{\alpha+1},t)\ , \tag{4.2}$$

where again $\tilde{C}$ stands for the structure factor that is symmetric between the second and third wave-vector components.

Since our model is coarse grained on a simple cubic lattice, we need to relate the structure factor defined through this model to that measured in the real experiment on a fcc lattice. The details are discussed in Appendix B and the two structure factors are related by (B10).

In the experiment in Ref. 9, Nagler *et al.* investigated the structure factor for the (100) superlattice peak, where $\mathbf{Q}=2\pi(1,0,0)$. They measured the profile of radial (parallel to $\mathbf{Q}$) and transverse (perpendicular to $\mathbf{Q}$) scans through the (100) peak. For radial scans,

$$\mathbf{Q}+\mathbf{q}=2\pi(1,0,0)+(q,0,0)=(2\pi+q,0,0)\ .$$

From (B10), we have

$$\tilde{C}_{\text{expt}}(2\pi+q,0,0)=4\tilde{C}_1(q,0,0)=4\tilde{C}(q;0,0)\ , \tag{4.3a}$$

where we have used Eq. (4.2) in the last equality. For transverse scans,

$$\mathbf{Q}+\mathbf{q}=2\pi(1,0,0)+(0,q,0)=(2\pi,q,0)$$

or

$$\mathbf{Q}+\mathbf{q}=2\pi(1,0,0)+(0,0,q)=(2\pi,0,q)$$

From Eq. (B10), we have

$$\tilde{C}_{\text{expt}}(2\pi,q,0)=4\tilde{C}_1(0,q,0)=4\tilde{C}(0;q,0)\ , \tag{4.3b}$$

and

$$\tilde{C}_{\text{expt}}(2\pi,0,q)=4\tilde{C}_1(0,0,q)=4\tilde{C}(0;q,0)\ . \tag{4.3c}$$

As will be shown later, $\tilde{C}(q;0,0)$ has a smaller peak width than $\tilde{C}(0;q,0)$.

The equation of motion (3.43) is nonlinear and in general can only be solved numerically. However, it can be solved analytically in certain limits. We first study the long-time scaling solution to (3.43) in the limit $a=0$. In this case, $C_1=C_2=C_3=C$ and C is isotropic,

$$C(\mathbf{R},t)=f_I(R/L)\ . \tag{4.4}$$

From (3.20), (3.32), and (3.43), we can write

$$\frac{\partial C(\mathbf{R},t)}{\partial t}=\nabla^2 C(\mathbf{R},t)+\frac{2}{L^2}C^{1/2}(\mathbf{R},t)\tan\left[\frac{\pi}{2}C^{1/2}(\mathbf{R},t)\right]\ . \tag{4.5}$$

Inserting (4.4) into (4.5), we obtain, following Mazenko, the scaling equation

$$-\mu\mathbf{x}\cdot\nabla_x f_I(x)=\nabla_x^2 f_I+2f_I^{1/2}\tan\left[\frac{\pi}{2}f_I^{1/2}\right]\ , \tag{4.6}$$

where $\mathbf{x}=\mathbf{R}/L$ and we assume $\mu=L(\partial L/\partial t)$ is a constant. If (4.6) holds for long times, then $L(t)\sim t^{1/2}$, as expected from the Lifshitz-Cahn-Allen[25] curvature-driven arguments. For small $\mathbf{x}$, expanding $f_I(x)$ in powers of x and matching the coefficients of x^n in (4.6), we obtain the solution

$$f_I(x)=1-\left[\frac{8}{\pi(d-1)}\right]^{1/2}x+\frac{6}{\pi(3d-1)}x^2+\cdots\ . \tag{4.7}$$

As pointed out by Oono[6] the linear term in (4.7) leads to Porod's law in Fourier space, $\tilde{C}(\mathbf{q},t)\sim q^{-(d+1)}$ for large q.

In the case $a\neq 0$, we look for the solution to (3.43) of the form

$$C_\alpha(\mathbf{R},t)=1-W_\alpha(\mathbf{R})/L \tag{4.8}$$

for $W_\alpha \ll L$. We find that W_a satisfies the time-independent equation

$$(\nabla^2+a\nabla_\alpha^2)W_\alpha=\frac{4}{\pi(W_{\alpha-1}-W_{\alpha+1}+W_\alpha)}+\frac{4}{\pi(W_{\alpha+1}-W_{\alpha-1}+W_\alpha)}\ . \tag{4.9}$$

For small a, (4.9) can be solved in power expansions of a. Let

$$W_\alpha=W_I+aW_\alpha^{(1)}+a^2W_\alpha^{(2)}+\cdots\ . \tag{4.10}$$

Equating both sides of (4.9) in powers of a, we obtain

$$\nabla^2 W_I=\frac{8}{\pi W_I}\ , \tag{4.11a}$$

$$\left[\nabla^2+\frac{8}{\pi W_I^2}\right]W_\alpha^{(1)}=-\nabla_\alpha^2 W_I\ , \tag{4.11b}$$

$$\left[\nabla^2+\frac{8}{\pi W_I^2}\right]W_\alpha^{(2)}=-\nabla_\alpha^2 W_\alpha^{(1)}+\frac{8}{\pi W_I^3}(W_{\alpha-1}^{(1)2}+W_\alpha^{(1)2}+W_{\alpha+1}^{(1)2}-2W_{\alpha-1}^{(1)}W_{\alpha+1}^{(1)}) . \tag{4.11c}$$

For very small $\mathbf{R}$, the solution to (4.11a)–(4.11c) is given by

$$W_I(\mathbf{R})=\left[\frac{8}{\pi}\right]^{1/2}a_0\left[1+\frac{1}{2d}\left[\frac{R}{a_0}\right]^2-\frac{1}{8d(d+2)}\left[\frac{R}{a_0}\right]^4+\cdots\right], \tag{4.12a}$$

$$W_\alpha^{(1)}=\left[\frac{8}{\pi}\right]^{1/2}a_0\left[-\frac{1}{2d}\left[\frac{R_\alpha}{a_0}\right]^2+\frac{1}{4d(d+2)}\left[\frac{R}{a_0}\right]^2\left[\frac{R_\alpha}{a_0}\right]^2+\cdots\right], \tag{4.12b}$$

and

$$W_\alpha^{(2)}=\left[\frac{8}{\pi}\right]^{1/2}a_0\left[\frac{1}{2d}\left[\frac{R_\alpha}{a_0}\right]^2-\frac{1}{8d(d+2)}\left[\frac{R_\alpha}{a_0}\right]^4-\frac{1}{4d(d+2)}\left[\frac{R}{a_0}\right]^2\left[\frac{R_\alpha}{a_0}\right]^2+\cdots\right] \tag{4.12c}$$

where from (3.19), (3.32), and (4.8), $a_0=\pi^{1/2}$. For large $\mathbf{R}$ (but $R\ll L$), we obtain

$$W_I(\mathbf{R})=2\left[\frac{2}{\pi(d-1)}\right]^{1/2}R , \tag{4.13a}$$

$$W_\alpha^{(1)}(\mathbf{R})=-\left[\frac{2}{\pi(d-1)}\right]^{1/2}R\cos^2\theta . \tag{4.13b}$$

$$W_\alpha^{(2)}(\mathbf{R})=\frac{1}{16}\left[\frac{2}{\pi(d-1)}\right]^{1/2}R(-11+22\cos^2\theta-5\cos^4\theta+4\sin^4\theta\sin^2\phi\cos^2\phi) , \tag{4.13c}$$

where the polar axis of the spherical coordinates is chosen along R_α direction. Inserting (4.13a)–(4.13c) into (4.10), we can write for large $\mathbf{R}$ (but $R\ll L$),

$$W_\alpha=2\left[\frac{2}{\pi(d-1)}\right]^{1/2}R\Phi_\alpha(\theta,\phi;a) \tag{4.14}$$

$$=2\left[\frac{2}{\pi(d-1)}\right]^{1/2}R\left[1-\frac{a}{2}\cos^2\theta+\frac{a^2}{32}(-11+22\cos^2\theta-5\cos^4\theta+\sin^4\theta\sin^2 2\phi)+\cdots\right], \tag{4.15}$$

where $\Phi_\alpha(\theta,\phi;a=0)=1$ and Φ_α depends on the angles θ and ϕ and the anisotropy parameter a. The general form (4.14) holds for any value of a while (4.15) only holds for small a ($\ll 1$). Equation (4.15) shows that (for small a) Φ_α is symmetric about $\theta=\pi/2$ plane, $\phi=\pi/4$ plane, and periodic in ϕ with period $\Delta\phi=\pi/2$. This agrees with the symmetry implied by (4.1). Φ_α increases from $\theta=0$ to $\pi/2$ for fixed ϕ and increases from $\phi=0$ to $\pi/4$ for fixed θ. For larger values of a, the above qualitative behavior remains valid, but the anisotropy will be stronger. Equation (4.15) agrees with (4.7) for $a=0$, leads to Porod's law, and demonstrates the anisotropic scaling of this model.

For very large $\mathbf{R}$ ($x=R/L\gg 1$) C_α becomes small and we can replace

$$\tan\left[\frac{\pi}{2}T_\alpha\right]\approx\frac{\pi}{2}T_\alpha . \tag{4.16}$$

Equation (3.43) is then linearized and can be written, for any value of a, as

$$\left[\frac{\partial}{\partial t}-\nabla'^2-\frac{\pi}{L^2}\right]C_\alpha(\mathbf{R}',t)=0 \tag{4.17}$$

where we have defined the primed R_α coordinate

$$R'_\alpha=\frac{R_\alpha}{(1+a)^{1/2}} , \tag{4.18}$$

and the primed Laplacian

$$\nabla'^2=\nabla^2+a\nabla_\alpha^2=\frac{\partial^2}{\partial R_{\alpha-1}^2}+\frac{\partial^2}{\partial R_{\alpha+1}^2}+\frac{\partial^2}{\partial R_\alpha'^2} . \tag{4.19}$$

The scaling solution to (4.17) is then given by

$$C(x')=C_0x'^{-(d-\pi/\mu)}e^{-\mu x'^2/2} , \tag{4.20}$$

where $x'^2=(R_{\alpha-1}^2+R_{\alpha+1}^2+R'_\alpha)/L^2$ and μ is defined below (4.6). Note that (4.20) implies that for large x the anisotropy simply corresponds to a dilation of the R_α component in space, which is not the case for intermediate x as shown in (4.15) for small a there is the ϕ dependence in addition to the θ dependence.

These analytical results can be shown to follow from the equation of motion (3.43) by a direct numerical solution. The computations were carried out on a simple cubic lattice of linear size 64. We take $\alpha=1$ in the computation and C_1 is symmetric between the R_2 and R_3 vari-

ables. Periodic-boundary conditions were used and symmetry was taken into account to reduce the computation time. We have tested the theory for several different initial conditions and have found that the long time results are independent of the initial conditions. We therefore study in detail the initial condition $S^2(t=0)=\epsilon_I=0.01$ and the anisotropy parameter $a=1.0$.

In Fig. 3, we show $S^2(t)\equiv C_1(\mathbf{R}=0,t)$ versus t, where $C_1(\mathbf{R}=0,t)$ is also equal to the volume under the peak of structure factor and is proportional to the total scattering intensity in the experiment. As can be seen, the behavior of $S^2(t)$ shows different regimes of growth from early to late times. Right after the quench, $S^2(t)$ relaxes for a very short period of time, the length of which is slightly longer for larger initial value ϵ_I. Following this delay $S^2(t)$ increases rapidly with time, and after a rapid rise, $S^2(t)$ begins to saturate and approach its equilibrium value $S^2(\infty)=1$. This behavior of $S^2(t)$ is in qualitative agreement with that of the integrated intensity for transverse scans in the experiment (Fig. 2 in Ref. 9). As will be discussed below, the growth regimes of fast rise and later slow equilibration of $S^2(t)$ can be distinguished by the line shapes of the structure factor. Scaling begins to hold during the later slow equilibration regime.

To characterize the domain growth, we use two different definitions of the characteristic domain size. One is defined by (3.32), denoted here as L_s, and the other is the cubic[26] root of the peak height of the structure factor, denoted as L_p,

$$L_p=\left[\frac{\tilde{C}_\alpha(\mathbf{q}=0,t)}{C_\alpha(\mathbf{R}=0,t)}\right]^{1/3}=\left[\frac{\int d^3R\, C_\alpha(\mathbf{R},t)}{C_\alpha(\mathbf{R}=0,t)}\right]^{1/3} \tag{4.21}$$

In Fig. 4, we show L_s and L_p versus $t^{1/2}$. As can be seen, L_p becomes a straight line after a short period of transient while L_s is a straight line only for the intermediate time window and then increases faster than the $t^{1/2}$ power law. This fast increase of L_s at long times is just due to the finite-size effect of the system (64^3 lattice). We have also tested this effect for smaller systems and the finite-size effect occurs at much earlier times. We have found that the finite size effect begins to appear when L_s is greater than one-half of the linear size of the system for $a=1$ and to appear earlier for larger values of a. From (3.32) and (4.21), we see that L_s is related to $C_\alpha(\mathbf{R}=0,t)$ while L_p is related to the sum of $C_\alpha(\mathbf{R},t)$. It is reasonable that L_s is more sensitive to the finite-size effect than L_p.

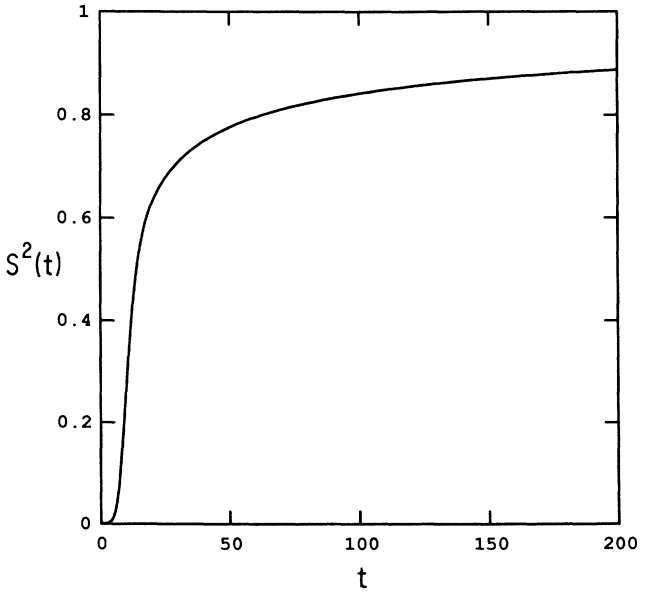

FIG. 3. Time dependence of $S^2(t)\equiv C_1(\mathbf{R}=0,t)$ up to $t=200$ after a quench for $a=1$ and $\epsilon_I=0.01$.

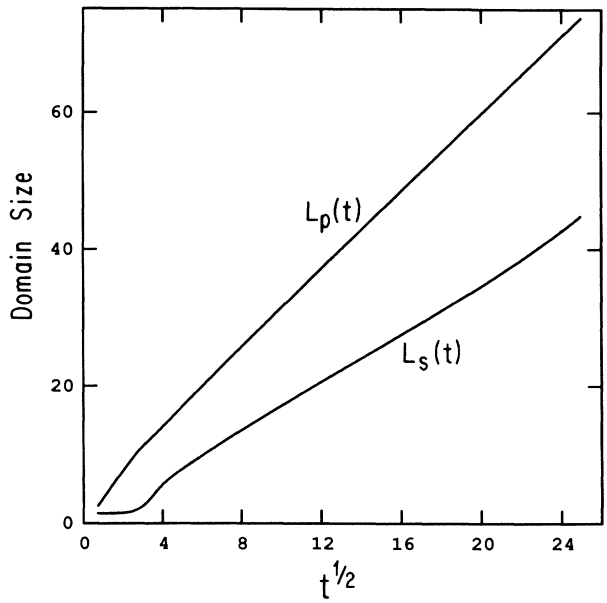

FIG. 4. The domain sizes $L_p(t)$ and $L_s(t)$ vs $t^{1/2}$ for $a=1$ and $\epsilon_I=0.01$.

We have studied the behavior of the correlation function and its Fourier transform—the structure factor. The structure factor at early times can be evaluated analytically. At early times, C_α is small and we can replace[27]

$$\tan\left[\frac{\pi}{2}T_\alpha\right]\approx\frac{\pi}{2}T_\alpha\ . \tag{4.22}$$

Thus the nonlinear terms in Eq. (3.43) and all those nonlinear terms ignored in the late stage theory can be linearized. The equation of motion can then be written as

$$\left[\frac{\partial}{\partial t}-(\nabla^2+a\nabla_\alpha^2)-B_2\right]C_\alpha(\mathbf{R},t)=0\ , \tag{4.23}$$

where B_2 is a positive constant. The solution, after Fourier transform, is given by

$$\tilde{C}_\alpha(\mathbf{q},t)=\tilde{C}_0 e^{-(q^2+aq_\alpha^2-B_2)t}\ . \tag{4.24}$$

For $q^2+aq_\alpha^2-B_2<0$, the peak grows exponentially with time. For a given time, the line shape is a Gaussian. In Fig. 5, we plot $\tilde{C}_1(\mathbf{q},t)$ versus q_2 and the Gaussian fit

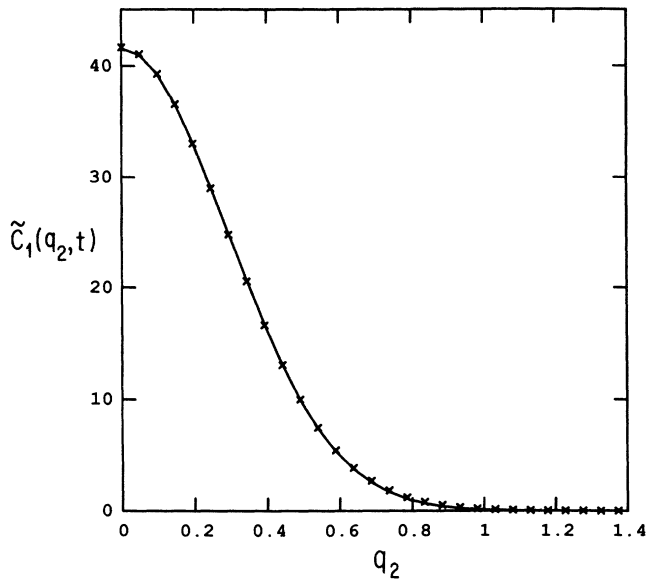

FIG. 5. The Gaussian fit of the early-time structure factor $\tilde{C}_1(\mathbf{q},t)$ vs $\mathbf{q}$ in q_2 direction for $t\approx 6$. The solid curve is the fit.

(solid curve) for $t\approx 6$ obtained from solving Eq. (3.43).

We have verified that the correlation function satisfies the anisotropic scaling in the long-time regime, which corresponds to the saturation regime of $S^2(t)$ shown in Fig. 3. In position space, the correlation function takes the following scaling form,

$$C_\alpha(\mathbf{R},t)=C_\alpha(\mathbf{R}=0,t)f_\alpha(\mathbf{R}/L_p(t)) , \tag{4.25}$$

where the scaling function $f_\alpha(0)=1$ and $f_\alpha(\mathbf{R}/L_p(t))$ is anisotropic in its argument. For $\alpha=1$, f_1 is symmetric between the R_2 and R_3 variables. In Fig. 6, we show the anisotropic scaling function $f_1(\mathbf{x})$ versus the scaled distance $\mathbf{x}=\mathbf{R}/L_p(t)$ in the R_1 (wide) and R_2 (narrow) directions. As can be seen, they have similar shapes, but different widths. If the curve for the R_1 direction is rescaled by a factor of $(1+a)^{1/2}=\sqrt{2}$, then these two curves *almost* fall on the top of each other. In Fig. 7 we show the scaling function f_1 versus the variables $x_1'=R_1/L_p(1+a)^{1/2}$ and $x_2=R_2/L_p$ for $a=4$, respectively. We easily see that after this rescaling of a factor of $(1+a)^{1/2}=\sqrt{5}$ the curve in R_1 direction becomes slightly narrower than that in R_2 direction. This means that as a increases the ratio of the widths in R_1 and R_2 directions becomes slightly smaller than the factor $(1+a)^{1/2}$. This also implies the more complicated dependence on the anisotropy parameter a than a dilation of (4.18). The behavior of the curves is consistent with the solutions given by (4.12a)–(4.12c), (4.15), and (4.20). For $x\sim 0$, the scaling function decreases with x^2 and after this, it decreases linearly with x for a region $0\ll x\ll 1$, which leads to Porod's law in Fourier space. For large x, our numerical analysis shows that the scaling function decays according to (4.20).

Again we have verified that the structure factor satisfies the following anisotropic scaling at relatively long times:

$$\tilde{C}_\alpha(\mathbf{q},t)=\tilde{C}_\alpha(\mathbf{q}=0,t)F_\alpha(\mathbf{q}L_p(t)) \\ =C_\alpha(\mathbf{R}=0,t)L_p^3(t)F_\alpha(\mathbf{q}L_p(t)) , \tag{4.26}$$

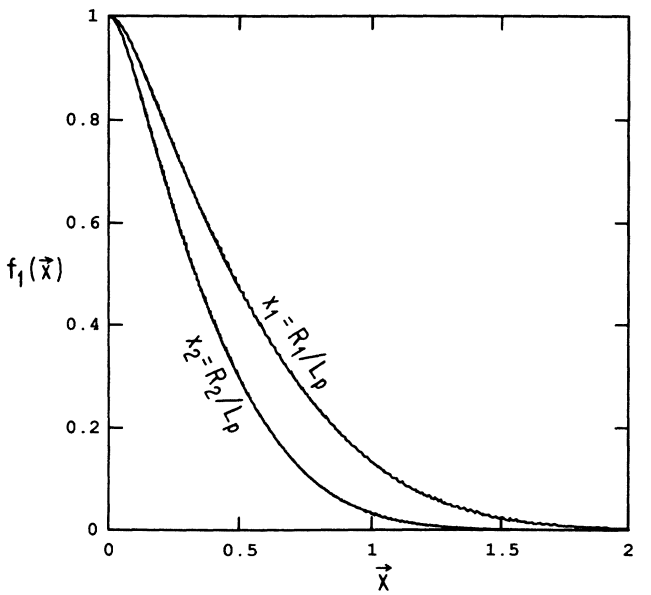

FIG. 6. In the position space the anisotropic scaling function $f_1(\mathbf{x})$ vs the scaled distance $\mathbf{x}=\mathbf{R}/L_p$ in R_1 (wide) and R_2 (narrow) directions for $a=1$. The wiggling of the curves represents the scaling of data at different times $t\approx 100$–300.

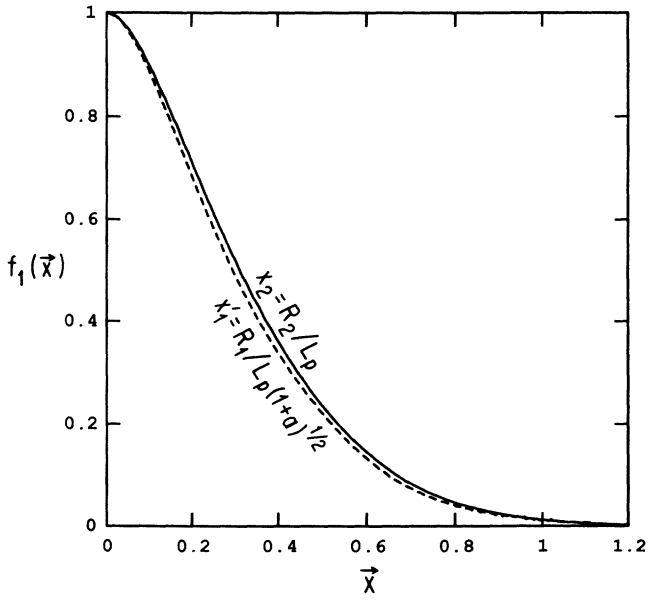

FIG. 7. In the position space the anisotropic scaling function $f_1(\mathbf{x})$ vs $x_1'=R_1/L_p(1+a)^{1/2}$ (dashed curve), and $x_2=R_2/L_p$ (solid curve) for $a=4$. Data are taken at $t\approx 100$ to avoid finite-size effect.

where $F_\alpha(0)=1$ and F_α is anisotropic in its argument. For $\alpha=1$, F_1 is symmetric between q_2 and q_3. In Fig. 8, we show the shape function F_1 versus the scaled wave number $\mathbf{k}=\mathbf{q}L_p(t)$ in the q_1 (narrow) and q_2 (wide) directions. Again, if the curve for q_1 direction is expanded by a factor $(1+a)^{1/2}=\sqrt{2}$, then these two curves *almost* fall on top of each other. From (4.3a) and (4.3b), we can identify the q_1 direction with the radial scan and q_2 direction with the transverse scan through the (100) peak in the experiment. Thus our theory indicates that the width of the radial scan should be narrower than that of transverse scan through the (100) peak, as is observed in the experiment in Ref. 9. The ratio of the widths of transverse to radial scans is slightly smaller[28] than $(1+a)^{1/2}$. If we extend the above discussion to (010), (001), and other superlattice peaks, using (B10) in Appendix B, we can generate similar ellipsoidal profiles of reflection in reciprocal space to that shown in Fig. 12.8 of Ref. 13. The ratio of the long axes of the ellipsoids to the short axes is slightly smaller than $(1+a)^{1/2}$. The experimentally observed[29] ratio of widths of transverse to radial scans varies from about 2.5 (quenched to lower temperature) to about 3 (quenched to higher temperature), showing some weak temperature dependence. If we use this ratio to estimate the anisotropy parameter a, this would correspond to $a=5-8$, which is very large anisotropy. If we use $a=5-8$ in our numerical computation, we need a system of $(1+a)^{1/2}$ larger in its linear size than the $a=0$ case to avoid the finite-size effect at relatively long times, which unfortunately is beyond our current computational ability. Hence we restrict ourselves to smaller anisotropy and a system of a linear size of 64 sites, but the qualitative features of the anisotropy dependence should not change for larger values of a.

We have found that the line shape in Fig. 8 can be approximately fitted to a modified Lorentzian-squared shape

$$F_1(k)=\frac{1}{(1+b_1k^2)^2+2b_2k^2}\ . \tag{4.27}$$

The fits for the curve in q_2 direction are shown in Fig. 9, where the solid curve represents the data and the dashed curve is the fit. For $a=1$, we obtain $b_1=0.087$ and $b_2=-0.046$. Equation (4.27) is consistent with that observed in the experiment and Porod's law for large k. We have tried to fit our data to Lorentzian-squared shapes as was done in Refs. 9 and 10, but the fits are inferior to (4.27). This could be due to the fact that the system has not completely settled into the longest time asymptotic regime for the size and time used in the computations. We have also fitted our data for large k to the following form:

$$F_1(k)=\frac{1}{1+bk^\beta}\ . \tag{4.28}$$

For the size and time used in the computations before observing the finite-size effect, we obtain the exponent $\beta\approx 4.3$, but still converging with time to the analytically obtained value of 4. The $\log_{10}$-$\log_{10}$ plot of fits are shown in Fig. 10. To obtain better quality data for the asymptotic shape function and to see more extended regions with Porod's tail numerically, we need larger systems and go to longer times. In Ref. 6, Oono pointed out that to demonstrate Porod's tail the linear dimension must be about 1000 sites in Monte Carlo simulations and 200–300

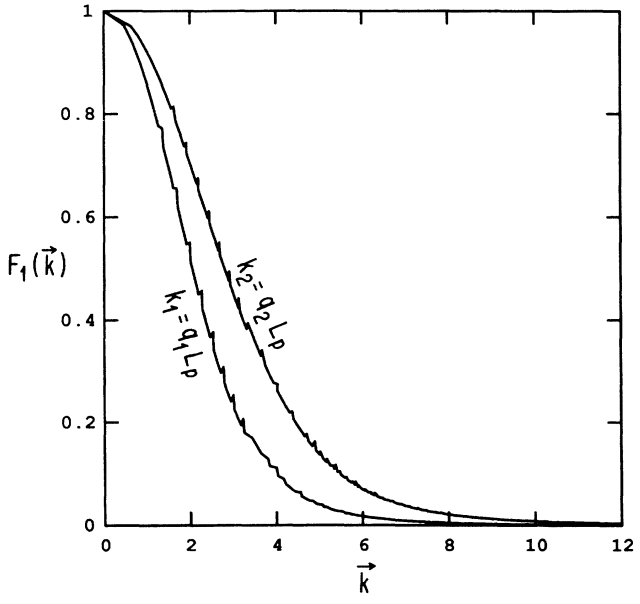

FIG. 8. In the wave number space the anisotropic shape function $F_1(\mathbf{k})$ vs the scaled wave number $\mathbf{k}=\mathbf{q}L_p$ in q_1 (narrow) and q_2 (wide) directions. The wiggling of the curves represents the scaling of data at different times $t\approx 100-300$. For a given time only a few data points with small $\mathbf{k}$ contribute to the peak shown.

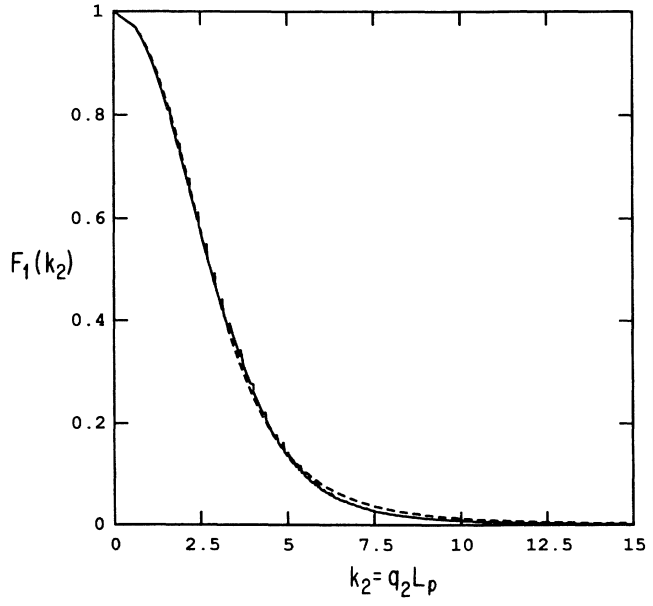

FIG. 9. The line shape in q_2 direction in Fig. 8 is fitted to the form of (4.27). The dashed curve is the fit.

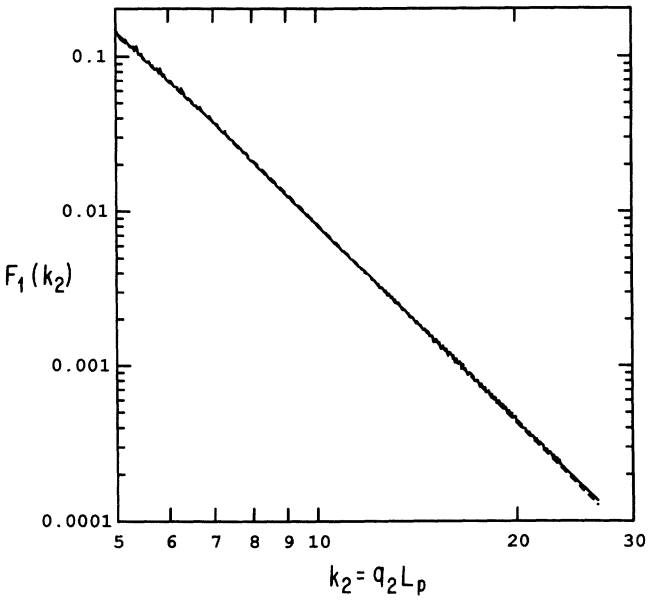

FIG. 10. The $\log_{10}$-$\log_{10}$ plot of the fit of the line shape in q_2 direction in Fig. 8 to the form of (4.28). The dashed curve is the fit.

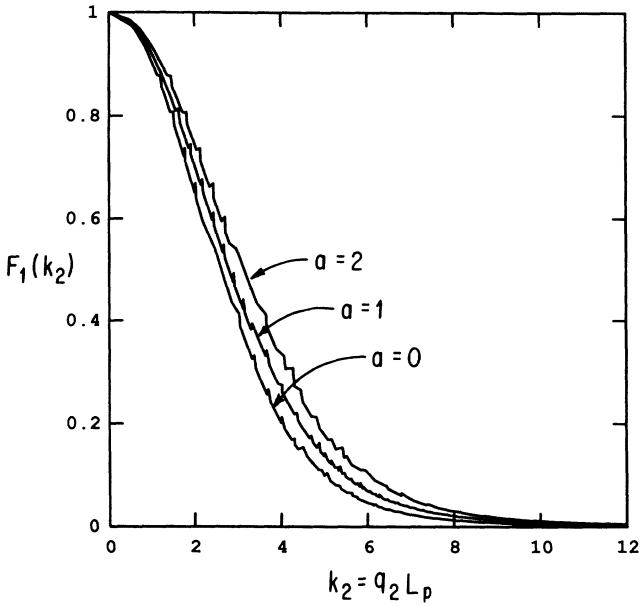

FIG. 12. In the wave number space the shape function $F_1(\mathbf{k})$ vs the scaled wave number $\mathbf{k}=\mathbf{q}L_p$ in q_2 direction for the anisotropy parameter $a=0$, 1, and 2.

sites in his cell dynamical system.

We have tested the theory for several values of the anisotropy parameter a. We plot in Fig. 11 the scaling function $f_1(\mathbf{x})$ versus $\mathbf{x}=\mathbf{R}/L_p$ in the R_2 direction for $a=0$, 1, and 2. As can be seen, in the position space the width decreases with a, but the shape remains the same. This verifies the more complicated dependence on the parameter a than a dilation of (4.18). In Fig. 12, we plot the shape function $F_1(\mathbf{k})$ versus $\mathbf{k}=\mathbf{q}L_p$ in the q_2 direction for $a=0$, 1, and 2. In the wave number space, the width increases with a, but the shape remains the same.

The model studied in this paper has a three-component order parameter and describes the ordering dynamics of Cu_3Au. An immediate question to ask is how the results of this model in the case $a=0$ (Ginzburg-Landau theory of the four-state Potts model[22]) differ from those of the

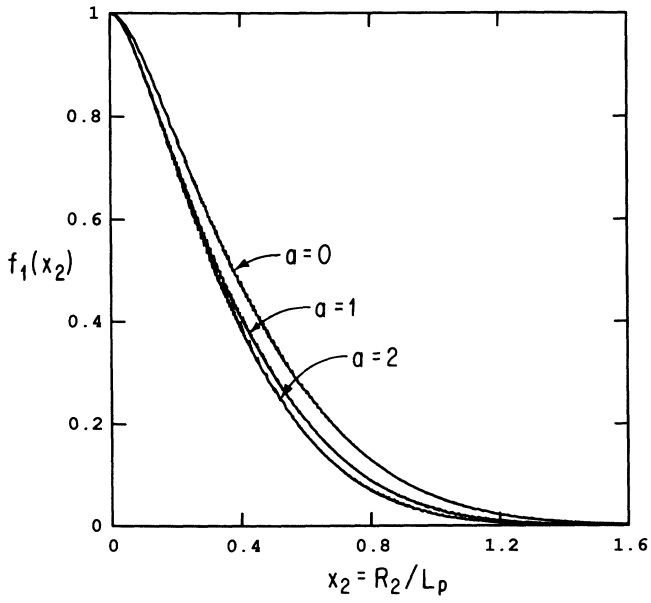

FIG. 11. In the position space the scaling function $f_1(\mathbf{x})$ vs the scaled distance $\mathbf{x}=\mathbf{R}/L_p$ in R_2 direction for the anisotropy parameter $a=0$, 1, and 2.

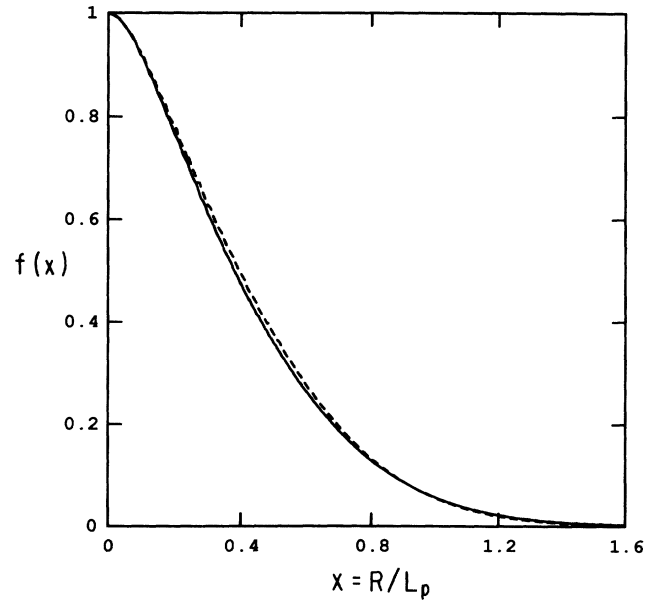

FIG. 13. In position space the scaling functions for Cu_3Au model for $a=0$ (solid curve) and for the scalar order parameter model (dashed curve) given by (4.29).

simpler scalar order parameter case (the two-state Potts model) studied by Mazenko in Ref. 7. The equation of motion for the nonconserved scalar order parameter, in the sharp interface limit, is given in Ref. 7 by

$$\frac{\partial C(\mathbf{R},t)}{\partial t}=\nabla^2 C(\mathbf{R},t)+\frac{2}{L^2}\tan\left[\frac{\pi}{2}C(\mathbf{R},t)\right], \quad (4.29)$$

where we have multiplied by a factor of 2 in the last term to compare with the Cu_3Au model in the case $a=0$. Comparing (4.5) with (4.29), we see that the two equations have different nonlinear terms. Following the discussion from (4.5) through (4.20), we can solve (4.29) in certain limits. The scaling solution for small x ($x=R/L$) in d dimensions is given by

$$C(\mathbf{R},t)=f(x)=1-\left[\frac{4}{\pi(d-1)}\right]^{1/2}x(1-\beta x^2)+\cdots, \quad (4.30)$$

where

$$\beta=\frac{1}{4d+2}\left[\frac{\pi}{3}+\mu\right].$$

For large x,

$$C(x)=C_0 x^{-(d-\pi/\mu)}e^{-\mu x^2/2}, \quad (4.31)$$

where μ is defined below (4.6). For very small R, we can write $C(\mathbf{R},t)=1-W(\mathbf{R})/L$ ($W\ll L$). Inserting $C(\mathbf{R},t)$ into (4.29), we obtain, for very small R,

$$W(\mathbf{R})=\left[\frac{4}{\pi}\right]^{1/2}a_0\left[1+\frac{1}{2d}\left[\frac{R}{a_0}\right]^2-\frac{1}{8d(d+2)}\left[\frac{R}{a_0}\right]^4+\cdots\right], \quad (4.32)$$

where $a_0=(\pi/2)^{1/2}$. Comparing the analytical results for both models, we immediately see that, while the x^2 term does not appear in (4.30) in the scalar order-parameter case, it survives in (4.7) in the Cu_3Au case. As was pointed out by Porod[5,30] for smooth interfaces, as in the scalar order-parameter case, with no angularities such as corners, edges, and vertices, the x^2 term does not appear. However, in the model for Cu_3Au special symmetries, which constrain σ_α to take the functional form of (3.38), may allow the existence of such angularities. On the other hand, both models lead to Porod's law and share similar results in very small R and very large R ($R/L\gg 1$) limits. Thus we would expect the scaling functions to differ only for intermediate x. To check the above arguments, we have solved (4.5) and (4.29) numerically. We found that, while the domain sizes $L(t)$ have different coefficients, the scaling functions only slightly differ numerically for intermediate $0<x<1$, as shown in Fig. 13.

V. CONCLUSIONS

In this paper we have constructed a coarse-grained model describing the order-disorder transition of Cu_3Au. The model is characterized by a Ginzburg-Landau Hamiltonian with a three-component order parameter and the symmetry of the Cu_3Au structure. This model differs from the usual $O(3)$ symmetric model in several important ways, and is a variant of the four-state Potts model. It takes into account two types of domain walls with spatial anisotropy. The equilibrium transition is first order rather than second order as in scalar order parameter case.

The ordering dynamics of this model subjected to a temperature quench are studied with Langevin dynamics, involving the generalization of the recently developed first-principles theory of unstable thermodynamic systems. Our theory explains the observed features in recent experiments on Cu_3Au. It shows qualitatively different physical regimes of growth from early to late times, which can be distinguished by the line shapes of the structure factor. The shape of the structure factor evolves from a Gaussian at early times to an approximately Lorentzian-squared shape at late times in the scaling regime. The model gives a growth exponent $n=\frac{1}{2}$, implying that the curvature-driven growth mechanism for a nonconserved scalar order parameter applies to the case with more than one type of walls and spatial anisotropy. However, these features lead to a structure factor exhibiting anisotropic scaling. The tail of the shape function obeys Porod's law.

ACKNOWLEDGMENTS

I am indebted to my advisor Professor Gene F. Mazenko for his guidance, encouragement, and support. I thank Dr. J. P. Lu for valuable discussions. I also thank Professor S. E. Nagler for explaining his group's experiments to me. I am grateful to Dr. J. F. Marko for a critical reading of the manuscript and comments. The computation time on Elxsi 6400 was granted by the Physical Sciences Division of the University of Chicago. This work was supported in part by National Science Foundation (NSF) Grant No. DMR-87-14707 and the Central Computer Facility of the NSF Materials Research Laboratory at the University of Chicago. This work was presented as a thesis to the Department of Physics of the University of Chicago in partial fulfillment of the requirements for the Ph.D. degree.

APPENDIX A: CORRECTIONS TO THE FUNCTIONALS

In Sec. III, we showed that the functional (3.9) does not lead to correct long-time scaling. In this appendix we discuss the corrections to (3.9), which better mimic the interfaces near $m\approx 0$ and restore the expected long-time scaling. The important point is that we require the corrections to cancel the term proportional to $[1-S(t)]$ in (3.37) to allow the

terms proportional to $[1-S(t)]^2$ in (3.37) to dominate at long times. This requirement can be satisfied if we choose the functional for σ_α in such a way that the multipoint correlation functions satisfy the following conditions at long times:

$$\psi_0^{-3}\langle\sigma_{\alpha-1}(1)\sigma_{\alpha+1}(1)\sigma_\alpha(2)\rangle=\psi_0^{-2}\langle\sigma_\alpha(1)\sigma_\alpha(2)\rangle-O[(1-S)^2] \tag{A1a}$$

and

$$\psi_0^{-4}\langle\sigma_\beta^2(1)\sigma_\alpha(1)\sigma_\alpha(2)\rangle=\psi_0^{-2}\langle\sigma_\alpha(1)\sigma_\alpha(2)\rangle-O[(1-S)^2]\ . \tag{A1b}$$

Using the equation of state, (2.6), we thus have

$$\left\langle\left[r\sigma_\alpha(1)+w\sigma_{\alpha-1}(1)\sigma_{\alpha+1}(1)+v\sigma_\alpha^3(1)+u\left[\sum_\beta\sigma_\beta^2(1)\right]\sigma_\alpha(1)\right]\sigma_\alpha(2)\right\rangle$$
$$=[r-w\psi_0+(3u+v)\psi_0^2]\langle\sigma_\alpha(1)\sigma_\alpha(2)\rangle-O[(1-S)^2]$$
$$=-O[(1-S)^2]\ , \tag{A2}$$

which is required by scaling. Guided by the above idea, we have found that we may choose the following functional:

$$\sigma_\alpha(\mathbf{R},t)=-\psi_0\tanh m_{\alpha-1}\tanh m_{\alpha+1}[1+\Theta(m_\alpha)]\ , \tag{A3}$$

where $\Theta(m_\alpha)$ must be an even function of m_α and vanishes as $m_\alpha\to\infty$ for (A3) to reproduce the correct ordered states. In particular, we choose

$$\Theta(m_\alpha)=\frac{A_1}{\cosh^2 m_\alpha}+\frac{A_2\tanh^2 m_\alpha}{\cosh^2 m_\alpha}+\frac{A_3\tanh^4 m_\alpha}{\cosh^2 m_\alpha}\ . \tag{A4}$$

where A_1, A_2, and A_3 are constants to be determined. Inserting (A3) into (A1a) and (A1b), we obtain the equations determining $\Theta(m_\alpha)$, to order $O(1/L)$,

$$\left\langle\frac{1}{\cosh^2 m}\right\rangle+\langle\Theta(m)\rangle=O\left[\frac{1}{L^3}\right]\ , \tag{A5a}$$

$$\left\langle\frac{1}{\cosh^2 m}\right\rangle+\left\langle\frac{\Theta(m)}{\cosh^2 m}\right\rangle=O\left[\frac{1}{L^3}\right]\ , \tag{A5b}$$

and

$$\langle[\Theta^2(m)+3\Theta(m)+2]\Theta(m)\rangle=O\left[\frac{1}{L^3}\right]\ . \tag{A5c}$$

Plugging (A4) into (A5a)–(A5c), after some algebra, we obtain $A_1=-2.4948$, $A_2=6.1981$, and $A_3=-2.8562$. This gives

$$\left\langle\left[r\sigma_\alpha(1)+w\sigma_{\alpha-1}(1)\sigma_{\alpha+1}(1)+v\sigma_\alpha^3(1)+u\left[\sum_\beta\sigma_\beta^2(1)\right]\sigma_\alpha(1)\right]\sigma_\alpha(2)\right\rangle$$
$$=-B[T_{\alpha-1}(12)K_{\alpha+1}(12)+T_{\alpha+1}(12)K_{\alpha-1}(12)]+O[(1-S)^3]\ , \tag{A6}$$

where

$$B=1.3503u\psi_0^2+v\psi_0^2+0.1775w\psi_0>0 \tag{A7}$$

and $K_\alpha(12)$ is defined by (3.15) and given by (3.36) in the sharp interface limit. The equation of motion (3.6) can then be written, to order $O(1/L^2)$ and at equal times $t_1=t_2=t$, as

$$\left[\frac{\partial}{\partial t}-2\Gamma_0 c_1(\nabla^2+a\nabla_\alpha^2)\right]T_{\alpha-1}(\mathbf{R},t)T_{\alpha+1}(\mathbf{R},t)-2\Gamma_0[T_{\alpha-1}(\mathbf{R},t)K_{\alpha+1}(\mathbf{R},t)+T_{\alpha+1}(\mathbf{R},t)K_{\alpha-1}(\mathbf{R},t)]=0\ .$$

APPENDIX B: RELATIONSHIP BETWEEN THE EXPERIMENTAL AND THEORETICAL STRUCTURE FACTORS

In this appendix we discuss the relationship between the experimental measured structure factor and that defined through this model.

The experimentally measured correlation function on the fcc lattice is

$$C_{\text{expt}}(\mathbf{r})=\langle s(\mathbf{r})s(\mathbf{0})\rangle\ , \tag{B1}$$

where $\mathbf{r}$ are fcc lattice sites, and spatial translational in-

variance has been used. Since the fcc lattice can be viewed as four interpenetrating simple cubic sublattices, we define the correlation function between two points on different simple cubic sublattices as

$$C_{i1}^{s}(\mathbf{R}+\mathbf{a}_{ij})=\langle s(\mathbf{R}+\mathbf{a}_{ij})s(\mathbf{0})\rangle \ . \tag{B2}$$

where $\mathbf{R}$ denotes simple cubic sublattice points, $\mathbf{a}_{ij}$ is one of the 16 possible basis vectors listed in Table I, and spatial translational invariance has been used. We can also define the correlation functions among the three components of the order parameter and the concentration as

$$C_{ij}^{\psi}(\mathbf{R})=\langle \psi_i(\mathbf{R})\psi_j(\mathbf{0})\rangle \tag{B3}$$

where $\psi_i=\{\psi_1,\psi_2,\psi_3,\Psi\}$.

The experimentally measured structure factor, with respect to a superlattice peak wave vector $\mathbf{Q}$, is then given by

$$\tilde{C}_{\text{expt}}(\mathbf{Q}+\mathbf{q})=\sum_{\mathbf{r}}^{\text{fcc}}\langle s(\mathbf{r})s(\mathbf{0})\rangle e^{i(\mathbf{Q}+\mathbf{q})\cdot\mathbf{r}} \ . \tag{B4}$$

The structure factor on the simple cubic sublattices can be defined by

$$\tilde{C}_{i1}^{s}(\mathbf{Q}+\mathbf{q})=\sum_{\mathbf{R}}^{\text{sc}}\langle s(\mathbf{R}+a_{ij})s(\mathbf{0})\rangle e^{i(\mathbf{Q}+\mathbf{q})\cdot(\mathbf{R}+\mathbf{a}_{ij})} \ , \tag{B5}$$

which is independent of the index j since $\mathbf{a}_{ij}$ are equivalent for fixed i and different j. The structure factor associated with the order parameters is given by

$$\tilde{C}_{ij}^{\psi}(\mathbf{q})=\sum_{\mathbf{R}}^{\text{sc}}\langle \psi_i(\mathbf{R})\psi_j(\mathbf{0})\rangle e^{i\mathbf{q}\cdot\mathbf{R}} \ . \tag{B6}$$

Since the fcc lattice can be viewed as four interpenetrating simple cubic sublattices, $\tilde{C}_{\text{expt}}(\mathbf{Q}+\mathbf{q})$ can be expressed in terms of $\tilde{C}_{i1}^{s}(\mathbf{Q}+\mathbf{q})$,

$$\tilde{C}_{\text{expt}}(\mathbf{Q}+\mathbf{q})=\sum_{\mathbf{R}}^{\text{sc}}\sum_{i=1}^{4}\langle s(\mathbf{R}+\mathbf{a}_{ij})s(\mathbf{0})\rangle \exp[i(\mathbf{Q}+\mathbf{q})\cdot(\mathbf{R}+\mathbf{a}_{ij})]=\sum_{i=1}^{4}\tilde{C}_{i1}^{s}(\mathbf{Q}+\mathbf{q}) \ , \tag{B7}$$

where $\tilde{C}_{i1}^{s}(\mathbf{Q}+\mathbf{q})$ is defined by (B5). We next want to express $\tilde{C}_{\text{expt}}(\mathbf{Q}+\mathbf{q})$ in terms of $\tilde{C}_{ij}^{\psi}(\mathbf{q})$ by making use of $\tilde{C}_{i1}^{s}(\mathbf{Q}+\mathbf{q})$. Using the definition of ψ_i, (2.2a)–(2.2d), and Table I, we can express $\tilde{C}_{ij}^{\psi}(\mathbf{q})$ in terms of $\tilde{C}_{i1}^{s}(\mathbf{Q}+\mathbf{q})$. For $\mathbf{q}$ near the superlattice ordering wave vector $\mathbf{Q}$, it is straightforward to show that

$$\tilde{C}_{11}^{\psi}(\mathbf{q})=\tfrac{1}{4}[C_{11}^{s}(\mathbf{Q}+\mathbf{q})-(-1)^{Q_1+Q_2}\tilde{C}_{21}^{s}(\mathbf{Q}+\mathbf{q})+(-1)^{Q_2+Q_3}\tilde{C}_{31}^{s}(\mathbf{Q}+\mathbf{q})-(-1)^{Q_3+Q_1}\tilde{C}_{41}^{s}(\mathbf{Q}+\mathbf{q})] \ , \tag{B8a}$$

$$\tilde{C}_{22}^{\psi}(\mathbf{q})=\tfrac{1}{4}[C_{11}^{s}(\mathbf{Q}+\mathbf{q})-(-1)^{Q_1+Q_2}\tilde{C}_{21}^{s}(\mathbf{Q}+\mathbf{q})-(-1)^{Q_2+Q_3}\tilde{C}_{31}^{s}(\mathbf{Q}+\mathbf{q})+(-1)^{Q_3+Q_1}\tilde{C}_{41}^{s}(\mathbf{Q}+\mathbf{q})] \ , \tag{B8b}$$

$$\tilde{C}_{33}^{\psi}(\mathbf{q})=\tfrac{1}{4}[C_{11}^{s}(\mathbf{Q}+\mathbf{q})+(-1)^{Q_1+Q_2}\tilde{C}_{21}^{s}(\mathbf{Q}+\mathbf{q})-(-1)^{Q_2+Q_3}\tilde{C}_{31}^{s}(\mathbf{Q}+\mathbf{q})-(-1)^{Q_3+Q_1}\tilde{C}_{41}^{s}(\mathbf{Q}+\mathbf{q})] \ , \tag{B8c}$$

$$\tilde{C}_{44}^{\psi}(\mathbf{q})=\tfrac{1}{4}[\tilde{C}_{11}^{s}(\mathbf{Q}+\mathbf{q})+(-1)^{Q_1+Q_2}\tilde{C}_{21}^{s}(\mathbf{Q}+\mathbf{q})+(-1)^{Q_2+Q_3}\tilde{C}_{31}^{s}(\mathbf{Q}+\mathbf{q})+(-1)^{Q_3+Q_1}\tilde{C}_{41}^{s}(\mathbf{Q}+\mathbf{q})] \ , \tag{B8d}$$

and

$$\tilde{C}_{ij}^{\psi}(\mathbf{q})=0, \quad \text{for } i\neq j \ , \tag{B8e}$$

where Q_1, Q_2, and Q_3 are three components of $\mathbf{Q}$. Equations (B8a)–(B8d) can be inverted to give

$$\tilde{C}_{11}^{s}(\mathbf{Q}+\mathbf{q})=\tilde{C}_{11}^{\psi}(\mathbf{q})+\tilde{C}_{22}^{\psi}(\mathbf{q})+\tilde{C}_{33}^{\psi}(\mathbf{q})+\tilde{C}_{44}^{\psi}(\mathbf{q}) \ , \tag{B9a}$$

$$\tilde{C}_{21}^{s}(\mathbf{Q}+\mathbf{q})=(-1)^{Q_1+Q_2}[-\tilde{C}_{11}^{\psi}(\mathbf{q})-\tilde{C}_{22}^{\psi}(\mathbf{q})+\tilde{C}_{33}^{\psi}(\mathbf{q})+\tilde{C}_{44}^{\psi}(\mathbf{q})] \ , \tag{B9b}$$

$$\tilde{C}_{31}^{s}(\mathbf{Q}+\mathbf{q})=(-1)^{Q_2+Q_3}[\tilde{C}_{11}^{\psi}(\mathbf{q})-\tilde{C}_{22}^{\psi}(\mathbf{q})-\tilde{C}_{33}^{\psi}(\mathbf{q})+\tilde{C}_{44}^{\psi}(\mathbf{q})] \ , \tag{B9c}$$

and

$$\tilde{C}_{41}^{s}(\mathbf{Q}+\mathbf{q})=(-1)^{Q_3+Q_1}[-\tilde{C}_{11}^{\psi}(\mathbf{q})+\tilde{C}_{22}^{\psi}(\mathbf{q})-\tilde{C}_{33}^{\psi}(\mathbf{q})+\tilde{C}_{44}^{\psi}(\mathbf{q})] \ . \tag{B9d}$$

Inserting (B9a)–(B9d) into (B7), we obtain

$$\begin{aligned}\tilde{C}_{\text{expt}}(\mathbf{Q}+\mathbf{q})=&\tilde{C}_{11}^{\psi}(\mathbf{q})[1-(-1)^{Q_1+Q_2}+(-1)^{Q_2+Q_3}-(-1)^{Q_3+Q_1}]\\&+\tilde{C}_{22}^{\psi}(\mathbf{q})[1-(-1)^{Q_1+Q_2}-(-1)^{Q_2+Q_3}+(-1)^{Q_3+Q_1}]\\&+\tilde{C}_{33}^{\psi}(\mathbf{q})[1+(-1)^{Q_1+Q_2}-(-1)^{Q_2+Q_3}-(-1)^{Q_3+Q_1}]\\&+\tilde{C}_{44}^{\psi}(\mathbf{q})[1+(-1)^{Q_1+Q_2}+(-1)^{Q_2+Q_3}+(-1)^{Q_3+Q_1}] \ .\end{aligned} \tag{B10}$$

Using (3.5) and ignoring the coupling between the ordering field σ_α and fluctuating field ϕ_α, we can decompose

$$\tilde{C}_{ii}^{\psi}(\mathbf{q})=\tilde{C}_{ii}^{\sigma}(\mathbf{q})+\tilde{C}_{ii}^{\phi}(\mathbf{q}) \ , \tag{B11}$$

in (B10).

*Present address: Department of Physics, University of Maryland, College Park, MD 20742.

[1]J. D. Gunton, M. San Miguel, and P. S. Sahni, in *Phase Transitions and Critical Phenomena,* edited by C. Domb and J. L. Lebowitz (Academic, London, 1983), Vol. 8; K. Binder and D. W. Heerman, in *Scaling Phenomena in Disordered Systems,* edited by R. Paym and A. Skjeltorp (Plenum, New York, 1985); H. Furukawa, Adv. Phys. **34**, 703 (1985); J. D. Gunton, *Time Dependent Effects in Disordered Materials,* edited by R. Pym (Plenum, New York, 1987).

[2]There is now vast literature on simulations of kinetic Ising models. These are reviewed in Ref. 1.

[3]R. Petschek and H. Metiu, J. Chem. Phys. **79**, 3443 (1985); O. T. Valls and G. F. Mazenko, Phys. Rev. B **34**, 7941 (1986); A. Milchev, K. Binder, and D. W. Heerman, Z. Phys. B **63**, 521 (1986); Y. Oono and S. Puri, Phys. Rev. Lett. **58**, 836 (1987); G. F. Mazenko and O. T. Valls, *ibid.* **59**, 680 (1987); T. M. Rogers, K. R. Elder, and R. C. Desai, Phys. Rev. B **37**, 9638 (1988); E. T. Gawlinski, J. Vinals, and J. D. Gunton, *ibid.* **39**, 7266 (1989).

[4]Z.-W. Lai, G. F. Mazenko, and O. T. Valls, Phys. Rev. B **37**, 9481 (1988).

[5]G. Porod, in *Small Angle X-Ray Scattering,* edited by O. Glatter and L. Kratky (Academic, New York, 1982).

[6]Y. Oono, Mod. Phys. Lett. B **2**, 861 (1988).

[7]G. F. Mazenko, Phys. Rev. Lett. **63**, 1605 (1989).

[8]G. F. Mazenko, O. T. Valls, and M. Zannetti, Phys. Rev. B **38**, 520 (1988).

[9]S. E. Nagler, *et al.*, Phys. Rev. Lett. **61**, 718 (1988).

[10]Y. Noda, S. Nishihara, and Y. Yamada, J. Phys. Soc. Jpn. **53**, 4241 (1984).

[11]By superlattice peaks we mean those diffraction peaks that are observed only when the system is in the ordered phase, but do not appear when the system is in the disordered phase, for example, the (100) peak for Cu_3Au system.

[12]R. Kikuchi and J. W. Cahn, Acta Metallur. **27**, 1337 (1979).

[13]B. E. Warren, *x-Ray Diffraction* (Addison-Wesley, Reading, 1969).

[14]S. C. Moss, in *Local Atomic Arrangements Studied by x-Ray Diffraction,* edited by J. B. Cohen and J. E. Hilliard (Gordon and Breach, New York, 1966).

[15]L. D. Landau and E. M. Lifshitz, *Statistical Physics* (Pergamon, London, 1980).

[16]J. Toledano and P. Toledano, *The Landau Theory of Phase Transitions* (World Scientific, Singapore, 1987).

[17]D. de Fontaine, in *Solid State Physics,* edited by H. Ehrenreich *et al.* (Academic, New York, 1979).

[18]This implies that ψ_α defined by (2.2a)–(2.2c) are coarse grained over the conventional unit cell of the fcc lattice. See, S.-k. Ma, *Modern Theory of Critical Phenomena* (Benjamin, Reading, Mass. 1976).

[19]Throughout the paper we develop the theory in the continuum formalism. The discretized theory on a lattice with spacing l is obtained by the replacements

$$\int d^d R \to \frac{1}{l^d} \sum_{\mathbf{R}} ,$$

where the sums run over the simple cubic sublattice vectors, and

$$[\nabla \psi_\alpha(\mathbf{R})]^2 = \frac{1}{2l^2} \sum_{\delta} [\psi_\alpha(\mathbf{R}+\delta) - \psi_\alpha(\mathbf{R})]^2 ,$$

$$\nabla^2 \psi_\alpha(\mathbf{R}) = \frac{1}{l^2} \sum_{\delta} [\psi_\alpha(\mathbf{R}+\delta) - \psi_\alpha(\mathbf{R})] ,$$

where the sum runs over nearest-neighbor lattice vectors.

[20]Throughout the paper we use d to stand for dimensionality although $d=3$ for Cu_3Au.

[21]G. F. Mazenko and M. Zannetti, Phys. Rev. Lett. **53**, 2106 (1984); Phys. Rev. B **32**, 4565 (1985).

[22]F. Y. Wu, Rev. Mod. Phys. **54**, 235 (1982); R, K. P. Zia and D. J. Wallace, J. Phys. A **8**, 1495 (1975).

[23]Here we follow the heuristic argument by Mazenko in Ref. 7.

[24]The actual form of $\Theta(m_\alpha)$ does not really matter as long as it leads to the required scaling for the equation of motion.

[25]I. M. Lifshitz, Zh. Eksp. Teor. Fiz. **42**, 1354 (1962) [Soviet Phys.—JETP **15**, 939 (1962)]; S. M. Allen and J. W. Cahn, Acta. Metall. **27**, 1085 (1979); J. Phys. (Paris) Colloq. **7**, C7-54 (1977).

[26]We use $d=3$ in the computations. The definition (4.21) becomes apparent from (4.26).

[27]Strictly speaking, we should linearize Eq. (3.6) for early time behavior. However, the linearization (3.44) is more apparent and gives the same equation of motion.

[28]The data in wave number space for $a=4$ show this trend. However, the quality of data in wave number space is not so good as that in position space. This ratio should be obvious as follows from the results in position space.

[29]S. E. Nalger (private communication).

[30]H. Tomita, Prog. Theor. Phys. **72**, 656, (1984); **75**, 482 (1986).